Title
Design and Synthesis of Nanostructured Materials for Flexible Lithium-Ion Battery

Author
Lu, Xing

Publication Date
2020

Peer reviewed|Thesis/dissertation

University of California
Los Angeles

Design and Synthesis of Nanostructured Materials for Flexible Lithium-Ion Battery

A dissertation submitted in partial satisfaction of the
requirements for the degree Doctor of Philosophy
in Chemical Engineering

by

Xing Lu

2020

ABSTRACT OF DISSERTATION

Design and Synthesis of Nanostructured Materials for

Flexible Lithium-Ion Battery

by

Xing Lu

Doctor of Philosophy in Chemical Engineering

University of California, Los Angeles, 2020

Professor Yunfeng Lu, Chair

In recent years, continuous progress in electronic devices, especially in wearable devices, has attracted surging attention from the consumer market. Therefore, flexible energy storage was developed to fulfill the needs of new flexible devices with ultra-lightweight and small volume. The very recent products and concepts such as touch screens, roll-up displays, wearable sensors, and even implantable medical devices have shown great potential in flexible applications because of their extreme convenience. However, the development of corresponding power sources largely

lags behind these emerging technologies of flexible devices.

Lithium-ion batteries (LIBs), owing to high energy density and high operating voltage, have been serving as an ideal power source for flexible devices. Nevertheless, direct implementation of commercial LIBs leads to irreversible deformation of structural integrity, short-circuiting or even severe explosion hazard. Such dilemma originates from the poor flexibility of electrode and electrolyte. For electrode side, current electrode sheets used in LIBs are manufactured by holding active material particles and conductive agents by a small weight fraction of polymeric binders. Such fragile electrode structure could easily lose electrical contact under physical deformation, leading to disintegrated electrode sheets, drastic degradations of electrochemical performance, and even safety issue due to internal short-circuiting. For electrolyte side, LIBs employ nonaqueous liquid electrolyte with high ionic conductivity and excellent electrode wettability. However, the drawbacks of such electrolyte system are also evident: poor ion selectivity, flammability, and leakage issue while being deformed render unsuitability of liquid electrolyte for flexible device application.

To fabricate flexible LIBs, the current state-of-the-art research employs two design strategies involving electrode structure. One popular strategy is constructing scaffolding structure using carbonaceous materials to function as supportive matrix for active materials. Given carbon nanotubes (CNTs) as an example, the CNTs possess remarkable electrical conductivity and mechanical strength (elastic modulus: 1 TPa, tensile strength: 100 GPa), which contribute to conductive and flexible electrodes as the high-aspect ratio of CNTs can serve as threading materials. Another strategy is rational architecture design of active materials that are conventionally particulate. For example, vanadium pentoxide nanowires can be readily fabricated into free-standing and binder-free electrode membrane. Nevertheless, the most of strategies above

still fall short of practicality due to reduced portion of active materials and consequently compromised energy density.

In comparison with the mobile liquid electrolyte, the emerging solid-state electrolytes could largely solve circumventing issues of ion selectivity, flammability and leakage. As one prevailing category, solid polymer electrolytes comprising polymers and lithium salts feature decent manufacturing flexibility. Meanwhile, their poor ionic conductivity (10^{-8} ~ 10^{-5}S cm^{-1}) could be ameliorated by gel polymer electrolytes with organic solvents (plasticizers) and/or inorganic solid fillers (e.g., SiO_2). Nevertheless, the non-conductive fillers block ion-transport pathways while allow partial electrical conduction, limiting the interfacial engineering and compatibility with electrodes.

In this dissertation, we tackle the aforementioned critical issues of flexible batteries in two aspects. Firstly, we design and synthesize flexible electrode from prospective of material and architecture. A novel cathode constructed by entangling networks of V_2O_5, CNTs and polytetrafluoroethylene (PTFE) is design and fabricated. Notably, the resulting flexible battery simultaneously achieves excellent mechanical strength (800 MPa young's module), superior cycle durability (86% retention after 1000 times bending) and intriguing capacity (300 mAh g^{-1} at 0.25C).

Furthermore, a Zr-based metal-organic-framework (MOF) possessing open-metal sites (OMSs) was used as the microporous filler to facilitate cation (Li^+) conduction in GPL. Compared with the state-of-the-art research, our work significantly enhanced t_{Li^+} of GLP from 0.39 up to 0.66 while maintained 1.5 mS cm^{-1} ionic conductivity. Notably, a reduced thermal activation energy (from 113 to 76 meV) was observed, suggesting diffusion energy barriers was eased by selective promotion of Li^+ conduction.

To conclude, flexible Li-ion batterie system research is still at early developing stage. Above

work provides rational design and improvement of the current FLIBs system in rather facile and cost-effective way. The methodology we proposed are hoped to bring further innovation toward FLIBs field and be extended to numerous applications in the future.

The dissertation of Xing Lu is approved.

Vasilios Manousiouthakis

Dante Simonetti

Qibin Pei

Yunfeng Lu, Committee Chair

University of California, Los Angeles

2020

To my parents F. Lu and HX. Jiang; my dear family members in U.S.; my beloved children Derrick Lu and Eric Lu.

Table of Contents

List of Figures

List of Tables

Acknowledgment

I remember once imagining what I'd be like in the future, when I get out of the plane in Tom Bradley international airport twelve years ago. I pictured myself with all the decent qualities that I could ever thought of, and I was excited to meet with all the uncertainties in my life.

But it turns out that I was not ready. Along with the bumpy roads while I was pursuing my American dream, I have my fair share of ups and downs. During this long journey, I have to reconstruct my perspective of views over and over again until they finally shape to who I am.

There were numerous people that supported me along the way, and I would not be able to finish my journey without them. I would like to present my special thanks to them.

First and foremost, my advisor and my life mentor, Professor Yunfeng Lu. I would like to express my most sincere gratitude to him for offering such precious research opportunities. He is such a great mentor that his passion for research and life never fades. However, despite of the scientific thinking and research skills. To me, it is his patience that lays the foundation of his teaching. His willing to wait, leaves space for slow runners like me to have opportunities to grow. All the research learning and works would not be possible without his support. It is truly my lucky to have him as my mentor.

I would like to thank my committee members, Professor Qibin Pei, Professor Vasilios Manousiouthakis, and Professor Dante Simonetti, for their valuable help and suggestion on my research and dissertation.

To my group members in UCLA, I would like to present a special thanks to Dr. Li Shen, Dr. Jianqiang Shen, Dr. Haiping Wu, and Dr. Zenan Yu for their advices and guidance on my projects. I was able to build up my research only because of their meticulous support and encourage. Professor Bin Xu, Dr. Zaiyuan Le, Dr. Fang Liu, Dr. Duo Xu, Dr. Gurong Shen, Dr. Xianyang Li,

Dr. Dejia Kong, Dr. Shengxiang Ma, Dr. Jesse Baucom, Dr. Wenyue Shi, Dr. Cheng Zhang, Dr. Ran Tao, Dr. Jie Ren, Zheng Cao, Xinru Li, Shilin Chen, Roxanne Castillo, Jinhui Xu, and Xinyi Tan, thanks for their patience helping me on my understanding of the research and their assistances on experiments. Their accompany lighten my journey in UCLA.

Finally, special thanks to both my families in mainland China and U.S. I am lucky to have you as my family and supporting me study abroad. I am deeply appreciated for all that you have done for me without even a little hesitate. It is your support that helps me get out of the obstacles on my road.

At last, to my beloved children, Derrick and Eric, your dad always loves you.

VITA

2010 – 2014 B.S., Department of Chemistry
Arizona State University

2015 – 2020 Graduate Researcher, Teaching Assistant, Graduate Division Award
Department of Chemical and Biomolecular Engineering
University of California, Los Angeles

Publications

1. **Xing Lu**, Haiping Wu, Dejia Kong, Xinru Li, Li Shen*, and Yunfeng Lu*. Facilitating Lithium-ion Conduction in Gel Polymer Electrolyte by Metal-Organic Frameworks. ACS Materials letters 2020 2(11), 1435-1441.
2. Ran Tao, Fan Li , **Xing Lu**, Fang Liu, Jinhui Xu, Dejia Kong, Chen Zhang, Xinyi Tan, Shengxiang Ma, Wenyue Shi, Runwei Mo*, Yunfeng Lu*. High-Conductivity-Dispersibility Graphene Made by Catalytic Exfoliation of Graphite for Lithium-Ion Battery. Advanced Functional Materials. (Accepted)
3. L. Shen,* X. Li, **X. Lu**, D. Kong, A. Fortini, C. Zhang, Y. Lu*. Semiliquid Electrolytes with Anion-Adsorbing Metal-Organic Frameworks for High-Rate Lithium Batteries. *Chemical Communication*. (Under review)
4. V_2O_5/CNT composite materials for flexible battery electrodes. (in preparation)

Chapter 1. Background

1.1 Introduction

1.1.1 Energy storage

In the past 300 years, human civilization has gone through a miraculous advance because of new forms of energy were explored. The rapid growth of economic today is inextricably linked with energy consumption. Nevertheless, we have entered a new historical period, where the traditional fossil fuels can no longer sustain. Every day, human society burns more than a million terajoules of energy, which is roughly 3000 times of the daily output of Palo Verde nuclear power plant in Arizona.[1] The amount of energy we are chewing down has reached all-time high in human history. The rapid demand growth in developing countries and the increasing impact on our living environment has pushed us to transform our way of utilized energy to more efficient way.

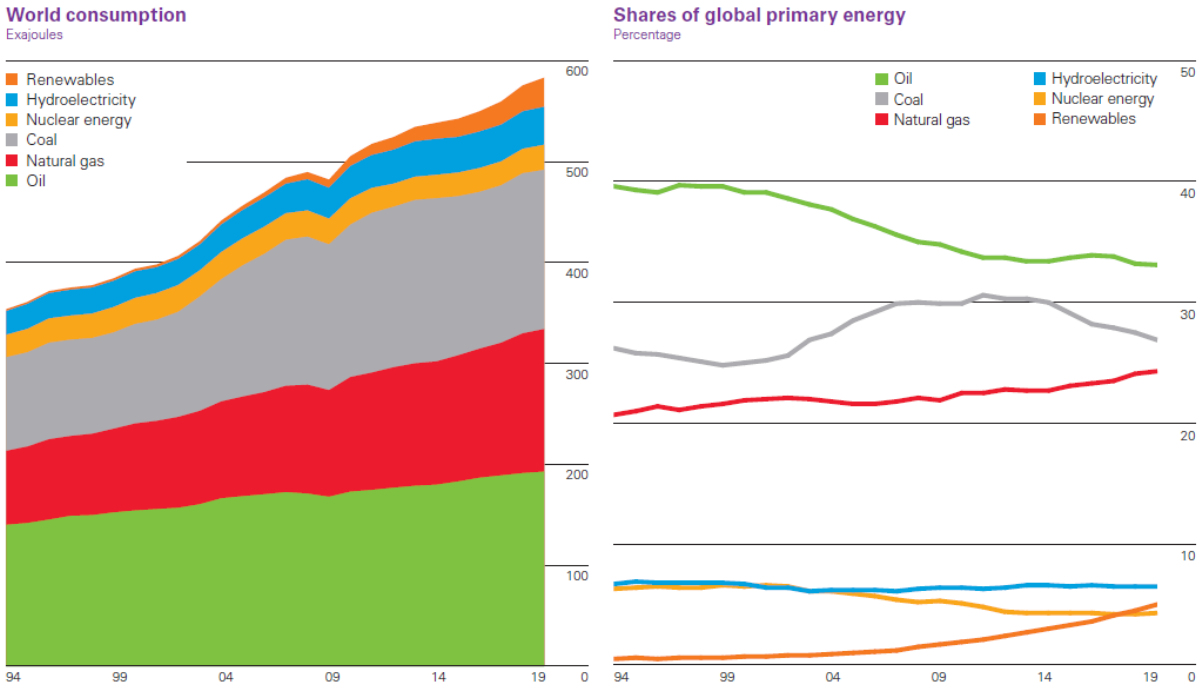

Figure 0-1. World Energy Consumption and shares of global primary energy.[2]

According to the Statistical Review of World energy 2020 report from BP[2], during the past

couple decades, along with the increasing consumption of the energy resources, the percentage of fossil resource usage kept decreasing while renewable energy started to overtake nuclear energy and makes up a huge portion of the energy consumption increase. Renewable energies such as solar power, wind power, and hydraulic power started to make more and more contribution to global primary energy shares. Nevertheless, direct utilization of different kinds of energy takes incredible efforts since their instability and complexity. Most of the renewable energy also shares a common drawback-discontinuity. Solar power and wind power for instance, can only be utilized during a certain period of time during a day.

Therefore, developing an efficient way of energy conversion and storage is important. The ultimate goal is to collect different forms of energy and keep them into a storage system that can be easily draw out and used without excess waste.

1.1.2 Electrochemical System

Thanks to tremendous amount of effort and research has been done in the past century, among all different kinds of energy conversion and storage systems, electrochemical system has been chosen as the most promising candidate due to its high efficiency. By using electricity as a median with chemical form of energy storage, the new era of renewable energy was able to be convert and storage in electrochemical system and transfer into electricity while we needed. Electrochemical storage system provides an environment friendly way to utilize energy in an efficient, stable, more flexible way via its chemical properties and variety of physical shapes.

There are many different types of electrochemical systems has been built during the last century. In order to distinguish them, the Ragone Plot has been developed. Using specific power and specific energy as parameter, electrochemical system can be evaluated with their

charge/discharge speed and their life span. As shown in the **Figure 1-2**, energy density means total amount of energy that can be stored inside of the system, and power density means the rate of energy transfer from the system.

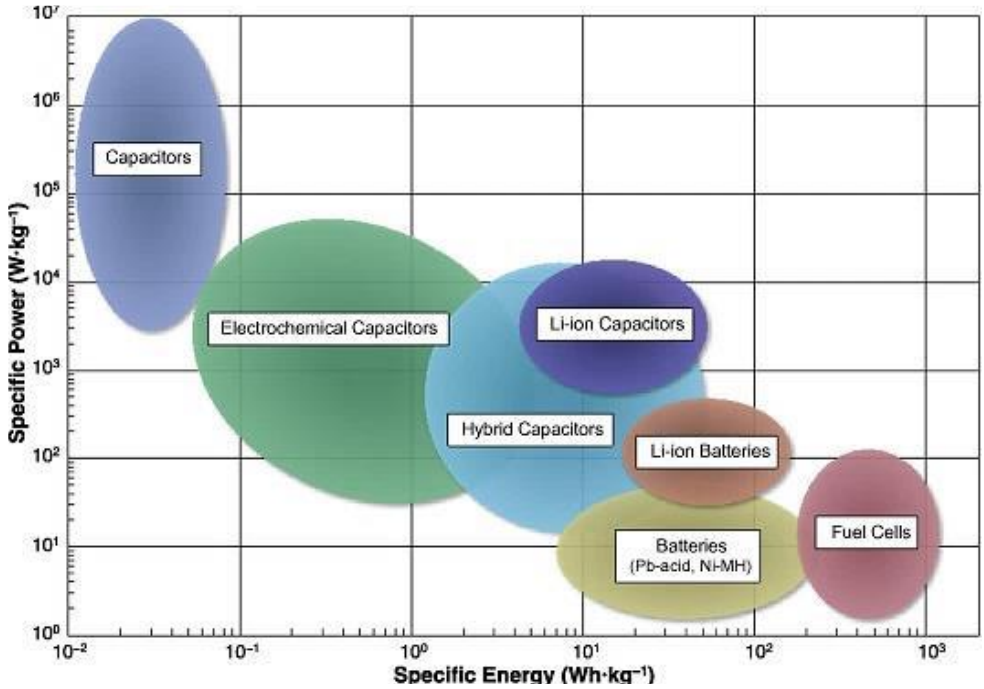

Figure 0-2. Energy-storage Ragone plot[3].

From the perspective of energy density, fuel cells obtain the highest specific energy which means they can have the most energy amount storage among all these systems. However, the current fuel cell technology is limited by its high requirement of working conditions and lack of safe storage solutions. In terms of power density, although the specific power of the capacitors can reach as high as 10^7W kg^{-1}, their relative energy density usually is about 30 times lower than practical cells, which is not enough to provide consistence usage in daily life. By comparison, electrochemical capacitors and batteries obtains the best energy-power density ratio which regarded as the best solution for electrical storage, especially battery category.

1.1.3 Basic concepts of electrochemistry and cell construction[4]

An electrochemical cell is the basic electrochemical unit that provides source of electrical energy by converting chemical energy into electric energy through electrochemical oxidation-reduction(redox) reaction. Each cell consists of components of anode, cathode, electrolyte and a separator. Electrochemical cell is connected either in series or parallel in order to provide required operating voltage and current levels. A cell can be viewed as two serially connected half-cells. Electrochemical cell can be easily divided into two main categories, primary battery and secondary batteries.

Primary battery is designed for generation of electrical energy until exhausted. Primary battery must be assembled in the charge state and discharge is the primary process during operation. Primary batteries cannot be recharged because their active materials cannot be returned to the original states hence the reactions are not reversible. Common types of primary batteries include Zinc-carbon batteries, alkaline batteries and lithium batteries. These batteries are designed for supplying high energy density, however, they are not suitable for wider applications because of the insufficient high-drain ability as well as serious environmental effect and tedious recycle procedure.

A secondary battery is a cell or group of cells for the generation of electrical energy in which the cell, after being discharged, may be restored to its original charged condition by an electric current flowing in the direction opposite to the flow of current when the cell was discharged. Other terms for this type of battery are rechargeable battery or accumulator. As secondary batteries are usually assembled in the discharged state, they must be charged first before they can undergo discharge in a secondary process. With better feasible manufacture cost and satisfying energy density, secondary batteries candidates such as Pb-acid, Ni-Cd, Ni-MH and lithium ion batteries

are popular to be used in electronic systems.

To define a good rechargeable battery, properties such as rate capability, cost, cycle life and temperature tolerance must be taken into consideration in any evaluation of a rechargeable battery. It is the improvement in energy density that has primarily driven the overall technological progress over the past 150 years — from lead–acid cells in the 1850s, nickel–cadmium cells in the 1890s and nickel metal hydride cells in the 1960s to, finally, lithium-ion batteries (LIBs) in the present day.[5]

1.1.4 Introduction to lithium-ion battery

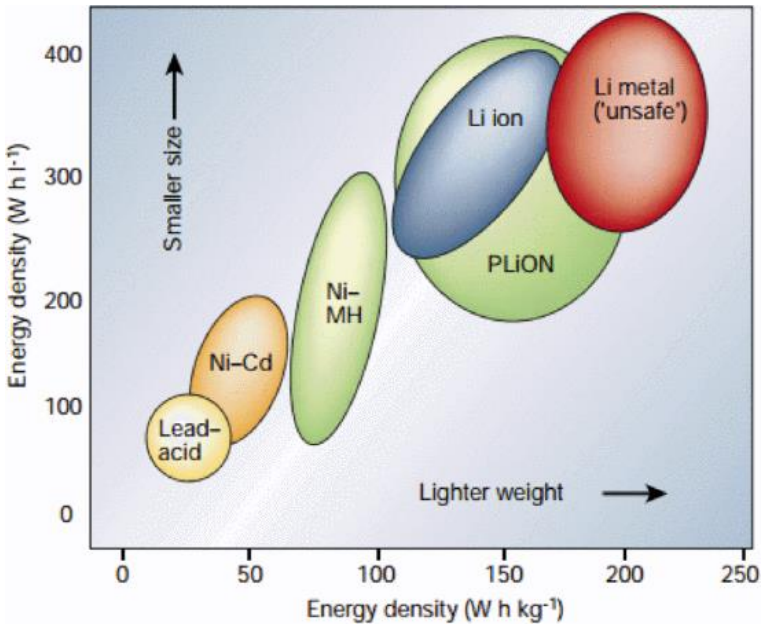

Figure 1.3 Different rechargeable battery systems comparison in terms of volumetric and gravimetric energy density.[6]

Although all secondary batteries are well-established technology, some intrinsic shortcomings

have hindered their widespread applications. According to Figure 1.3, for instance, utilization of Pb-acid and Ni-Cd batteries is limited by relatively low energy density. Commonly used Ni-MH battery only achieves an energy density of half of the Lithium ion (Li-ion) battery. These batteries are hindered by their relatively low energy density hence they can hardly be fabricated with lightweight or small size. However, it does not mean higher energy density is better. The only candidate that can achieve the highest energy density in rechargeable battery systems-Li metal battery, suffers from safety issues that also hindered its potential use in electronic devices.

Among all various existing technologies (Fig.1.3), lihtium-ion batteries currently outperform all other systems, occupying ~63% of worldwide sales values in portable batteries. Lithium-ion batteries (LIBs), as the main power source, dominate the electronic device market due to their high energy density, high output voltage, long-term stability and environmentally friendly operation.

Firstly, lithium has the lowest reduction potential compare with other elements, allowing Li based batteries to have the highest possible working voltage. Second, Li is the lightest metallic element and has the smallest ionic radii in any single charged ions. These advantages allow Li-based batteries to acquire high volumetric and gravimetric energy density and power density. Lastly, although multivalent cations afford for higher charge capacity, the additional charge severely decreases their mobility. Known that ionic diffusion in the solid electrodes is often the rate-limiting issue for power performance, this offers a giant obstacle for the further development of such alternative chemistries.

Considering of the combination of high energy and power density, lithium-ion battery was able to fulfill most of our daily used electronic appliances such as cell phones, laptops, or earphones with rather small battery size. In addition to small appliances, lithium-ion batteries also became the technology of choice for larger energy storage system because of sufficient power

density. Instead of conventional combustion engine, it provided a good alternative choice for large Electrical Vehicles (EVs) and UPS systems (uninterruptable power supply). Therefore lithium-ion battery is of intense interest from both research and consumer markets in recent years.

1.1.5 Battery mechanism and thermodynamics

A lithium-ion battery consists of three functional components, the anode (negative electrode), cathode (positive electrode) and electrolyte (Fig. 1.4). When the battery is discharged, lithium ions move from anode to cathode through the non-aqueous electrolyte, carrying the current. During charging, an external electrical power source forces the current to pass in the reverse direction and make lithium ions migrate from the cathode to the anode across the electrolyte. Separator is placed between the cathode and anode in a lithium-ion battery in order to prevent the physical contact of electrodes and allow ionic transport.

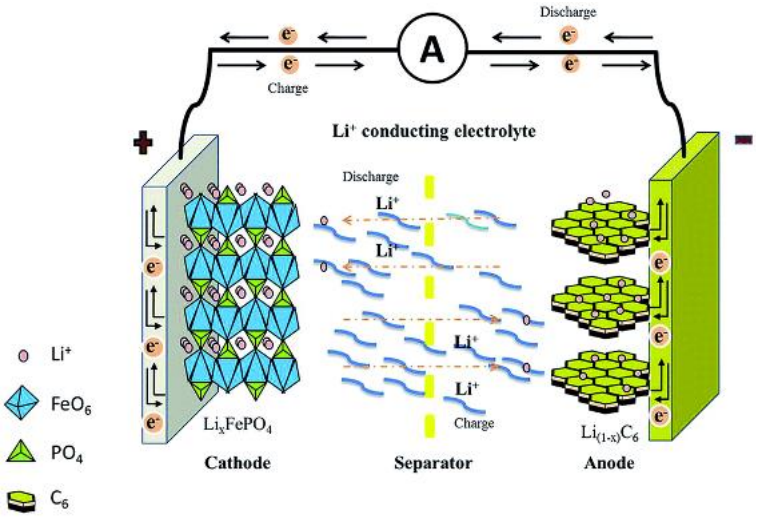

Figure 1.4 schematic illustration of a LiFePO4 lithium-ion battery[7]

Given a reversible LiFePO4 cell as an example to illustrate these two processes, where $Li_{(1-}$

$_{x)}C_6$ serves as anode and LixFeO4 is used as cathode material. The discharge reaction can be written as follows:

Negative electrode:

$$6C + xLi^+ + xe^- \underset{\text{Discharge}}{\overset{\text{Charge}}{\rightleftharpoons}} Li_xC_6$$

Positive electrode:

$$LiFePO_4 \underset{\text{Discharge}}{\overset{\text{Charge}}{\rightleftharpoons}} Li_{1-x}FePO_4 + xLi^+ + xe^-$$

The overall reaction can be expressed as:

$$LiFePO_4 + 6C \underset{\text{Discharge}}{\overset{\text{Charge}}{\rightleftharpoons}} Li_{1-x}FePO_4 + Li_xC_6$$

The storage electricity or capacity of a cell is determined by the amount of active materials in the electrode. It is expressed as the total quantity of electricity produced in the electrochemical reaction and is defined in terms of coulombs or ampere-hours.

1.1.6 Considerations of battery parameters

1) Theoretical specific capacity[8]

For a given redox electrode reaction, the theoretical specific gravimetric capacity can be calculated based on the following equations:

$$nZF = It\ (Farady's\ law)$$
$$Q_{theoretical} = \frac{zF}{3.6M}\ (mAh\ g^{-1})$$

n: amount of active material (mol);

z: amount of electron involved per molar active material;

F: Farady constant (9.65×10^4 C/mol, A·s/mol));

M: molar mas of active material (g/mol);

2) Energy density

The specific energy (energy per unit weight) can be obtained by measuring the time $\Delta t_{discharge}$ for its complete discharge under constant current $I_{dis} = dQ/dt$:

$$E = \int_0^t VIdt = \int_0^q V\,dQ\ (Wh\ kg^{-1})$$

The energy density (energy per unit volume) can be calculated by $E \cdot \rho$, where ρ is the tap density or packing density for electrode materials.

3) Coulombic efficiency

Coulombic efficiency can be calculated as follows:

$$E = \frac{Q_{discharge}}{Q_{charge}}\ (\%)$$

The Coulombic efficiency is primarily induced by irreversible process due to parasitic reactions, like electrolyte decomposition and SEI formations. Unstable SEI layer with electrolyte-permeable defects or cracks would result in continuous consumption of electrolyte and deterioration of battery calendar life.

1.1.7 Current state of art of lithium ion battery materials.

At present lithium-ion batteries (LIBs) are one of the most promising candidates for power sources of flexible devices because of their high energy density, large power density and long-term stability. Each LIBs consist of different components including current collector, active material, separator, electrolyte, packaging materials and adhesives. The selection, assembly of electrode materials, separator and packaging are central issues in developing high performance flexible LIBs.

Searching for higher power and higher energy density within lithium ion batteries is endless. Most of the research efforts are devoting in electrode materials, which intrinsically determine the energy and power density, as well as the cycling performance of the cell.

1.1.7.1 Cathode materials

A LIBs cathode has a solid host network which is able to store guest Li^+ ions. This so-called intercalation process allows guest Li^+ ions both inserting and escaping from the cathode side reversibly. All LIBs cathode materials are consisting of metal chalcogenides, transition metal oxides, and polyanion compounds which can be distinguish into difference crystal structures such as spinel, layered, olivine and tavorite (Figure 2.1).

Lithium cobalt oxide ($LiCoO_2$) is the most famous cathode material which is discovered by Goodenough in 1980. It was first commercialized by SONY, and remains as one of the majorities of commercial LIBs battery market. It has layered structure with a practical capacity of 140 mAh g^{-1}. However, only about 0.5 Li can be utilized in $LiCoO_2$, which brought the theoretical capacity of 273mAh/g to its half. When Li content is extracted above 0.5 in $Li_{1-x}CoO_2$, the transition from hexagonal to monoclinic phase will occur, leading to severe capacity fading and drastic exothermic reaction with organic electrolytes. Figure 2.1 (a) shows the structure of $LiCoO_2$. It has high energy density, high electronic and Li+ ion conductivity. The practical specific energy is 150 Wh kg^{-1} with graphite as anode.

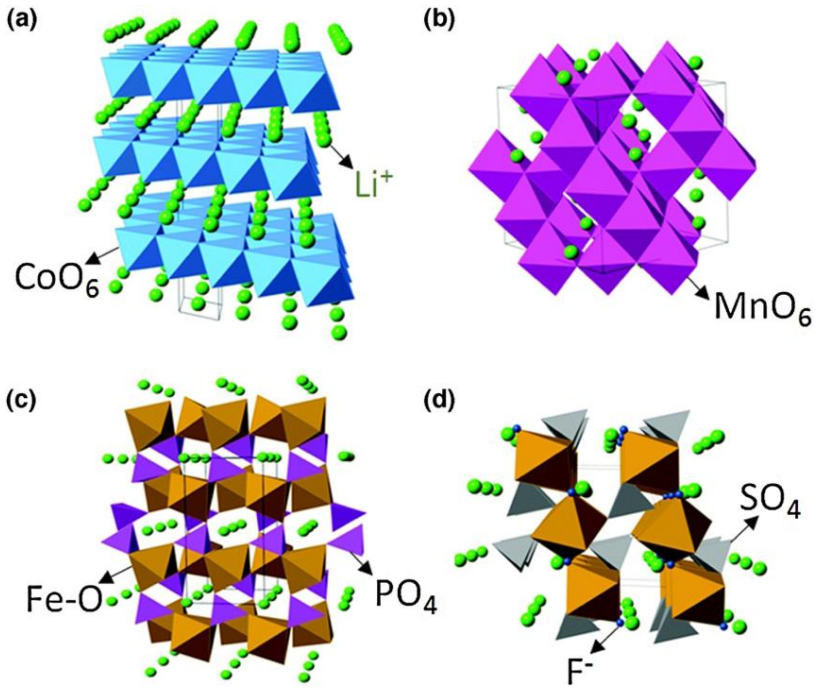

Figure 1.5 Crystal structures and discharge profiles of representative intercalation cathodes: structure of (a) layered ($LiCoO_2$), (b) spinel ($LiMn_2O_4$), (c) olivine ($LiFePO_4$), and (d) tavorite ($LiFeSO_4F$) (reproduced with permission Copyright (2014) Royal Society of Chemistry.) [9, 10]

Unlike $LiCoO_2$, $LiMn_2O_4$ obtains more stable structures that would not change easily during the lithium ion insertion and extraction. The stable structure of $LiMn_2O_4$ provides better safety and

rate performance. However, its low cycling life and capacity still hindered the overall performance of the material. Figure 2.1 (b) shows the crystal structure of $LiMn_2O_4$, the strong edge-shared octahedral structure allows reversible extraction of Li^+ ions from tetrahedral sites without affecting $[Mn_2]O_4$ spinel framework.

The structure of $LiFePO_4$ is shown in Figure 2.1 (c) and falls into the category of olivines, consisting of a distorted hexagonal close-packed (hcp) oxygen framework with 1/8 of the tetrahedral holes occupied by P, and 1/2 of the octahedral holes occupied by various metal atoms (in this case Li and Fe). Layers of FeO_6 octahedral are corner-shared in the b-c plane and linear chains of LiO_6 octahedral are edge-shared in a direction parallel to the b-axis. These chains are bridged by edge and corner shared phosphate tetrahedral, creating a stable three-dimensional structure. Due to its unique structure property, $LiFePO_4$ obtains superior safety and cycling performance compare to $LiCoO_2$ and $LiMn_2O_4$. Nevertheless, the low cell voltage became the weakest point of this material and stand in the way to improve its capacity.

1.1.7.2 Anode materials

Anode is another essential part to fabricate a full LIB. As an anode material, Lithium (Li) metal was first used for rechargeable batteries because of its high theoretical specific capacity (3860 mAh g^{-1}), low density (0.59 g cm^{-3}) and lowest negative electrochemical potential (-3.040V).[11] However, the uncontrollable growth of lithium dendrite hindered the coulombic efficiency hence further limited its actual applications. Compare to lithium metal batteries, conventional LIBs anode used Graphitic and hard carbons in order to reduce the forming of lithium dendrites, hence higher battery safety. Li^+ ions can be insert easily between the graphene layers, provides a good reversible intercalation (Figure2.2). Graphite has dominated the LIBs market because of its low cost,

abundant availability, high electrical conductivity and high Li^+ transportation.

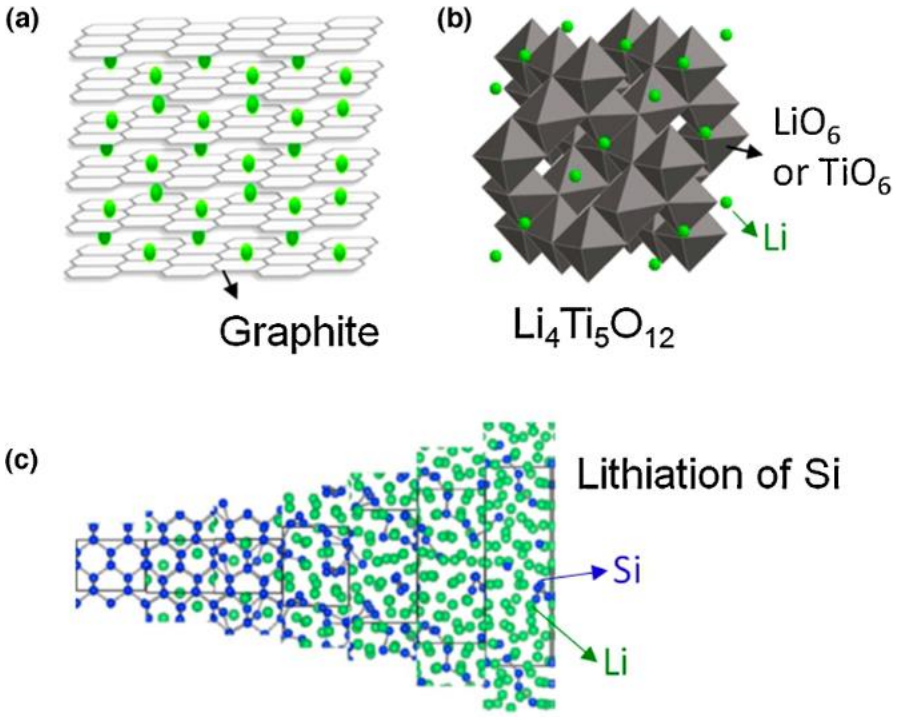

Figure 1.6 Crystal structures of (a) lithiated graphite,[12] (b) lithium titanate (LTO),[13] and (c) silicon during lithiation (reproduced with Permission Copyright (2014) American Chemical Society) [14]

Despite carbon-based materials, lithium titanium oxide ($Li_4Ti_5O_{12}$/LTO) has also been successfully commercialized (Figure1.6b). Although LTO obtains relative low cell voltage and capacity(175mAhg^{-1}), its high cycling life and high rate performance still make a good choice for batteries. Because of its highly stable lithiation/delithiation mechanism, LTO can restrain its volume change to a minimum amount (0.2%). A high equilibrium potential (~1.55V vs. Li/Li^+) of LTO also allows the potential window to reach above 1 V, which can reduce SEI growth and increase SEI stability, hence leading to high rate performance and preventing dendrite formation. Therefore, LTO is considered as promising anode material for high power, high cycling life LIBs.

Among different types of anode materials, alloying materials that forms with lithium metal can obtain extremely high volumetric and gravimetric capacity. Given silicon as example (Figure 1.6c), most of the alloying materials suffer from large volume change during the charge/discharge process, which leads to fracture in active materials and poor electrical contact. Therefore, even though Si has relatively low average delithiation potential and high gravimetric capacity, its high-volume change has prevented it from becoming a practical battery use.

1.1.7.3 Electrolyte materials

Current electrolytes in commercialized LIBs are mostly liquid non-aqueous electrolytes that consist of different types of lithium salts ($LiPF_6$/$LiBF_4$/$LiClO_4$) with organic solvents (EC/PC/DMC/EMC/DEC) and additives. The advantages of liquid electrolyte are due to its high wettability and ionic conductivity (10mScm^{-1} in ambient temperature). In table 1-1, the physicochemical properties of common solvents are listed.

Table 1-1. The physicochemical properties of some common solvents.[15]

Solvent	**FW**	***d*, g cm^{-3} (25 °C)**	**ε_r (25 °C)**	**η, mPa s (25 °C)**	**E_{homo}, eV**	**E_{lumo}, eV**	**mp, °C**	**bp, °C**	**fp, °C**
Ethylene carbonate (EC)	88	1.32 (40 °C)	90 (40 °C)	1.9 (40 °C)	−12.86	1.51	36	238	143
Propylene carbonate (PC)	102	1.2	65	2.5	−12.72	1.52	−49	242	138
Dimethyl carbonate (DMC)	90	1.06	3.1	0.59	−12.85	1.88	5	90	17
Ethyl methyl carbonate (EMC)	104	1.01	3	0.65	−12.71	1.91	−53	108	23
Diethyl carbonate (DEC)	118	0.97	2.8	0.75	−12.59	1.93	−74	127	25

As the solvents in LIBs electrolytes, most of them are highly volatile and flammable agents. Therefore, in recent years, instead of developing higher electrical performance, attentions started switching to find solid-state/semi-solid-state electrolytes for better safety battery operations.

1.2 Flexible batteries

Many attempts have been tried to make battery flexible during the past decade. There are three main strategies: 1) replacing conventional components with deformable materials; 2) optimizing fabrication processes; 3) design new device structures. Among all three strategies, replacing components are being focused the most to construct flexible/stretchable batteries.

1.2.1 CNT-based materials for flexible LIBs. [16]

Flexible electrode materials are core component to fabricate flexible LIBs. The main electrode materials for flexible LIBs are membrane like carbon-based materials, including CNTs, graphene and carbon cloth/textile. CNTs are one-dimensional (1D) carbon materials which are one of the core components for constructing flexible LIBs. The electrical conductivity of CNTs can be as high as 2×10^5 S cm^{-1}. CNTs have an elastic modulus of approximately 1 TPa and a tensile strength of approximately 100 GPa. These performances make CNTs a very good material to construct flexible electrodes. Due to its structure, CNTs allowed high fault tolerance since different current pathways are enabled while there are disconnections or missing links. Their high aspect ratio, low density, chemical stability, high electrical conductivity and mechanical flexibility allowed them to be applied into flexible membranes with all different kinds of methods such as vacuum filtration, dry-drawing, self-assembly, blade-coating, and so on. To elaborate the structural design of the flexible battery electrodes, building free-standing CNT-based membrane would provide reduced

weight, better flexibility and conductivity.

1.2.1.1 CNT-based anode materials for LIBs

Flexible electrode can be achieved through using CNT flexible membrane as both electrode and current collector materials. For instance, Li et al. recently brought out an unique route by coating the CNT film on commercial separator by filtration method so flexible anode can be obtained directly.[17] This method was achieved with free-standing single wall CNT/double-wall CNT and multi-wall CNT papers that were synthesized by vacuum filtration. The mechanical strength and flexibility of this integrated electrode have been greatly improved because the separator is a necessary component of LIBs. The absence of the binder and metallic current collector increases the energy density. Compare to electrodes made from casting CNTs on Cu current collector, the flexible electrode was able to obtain higher capacity, better rate capability and cycling stability. The disadvantage of the method is the small thickness (1um) of the active material, which limits the total energy of the cell. The capacity of the cell drops significantly decreases while the thickness increases from 1 to 6 um as well. In addition, the presence of the surfactants can be adsorbed on the surface of the CNTs and reduce the electrical conductivity.

Other than vacuum filtration method, chemical vapor deposition (CVD) self-assembly is also being used to obtain flexible CNT membranes. In this specific method, surfactants can be avoided. For example, CNT/CL(highly conductive carbon layer paper) composite can be synthesized through direct CVD growth and show reversible capacity of 572mAhg^{-1} after 100 cycles at 0.2 mA cm^{-2}. [18]

Aligned CNT (ACNT) array was also used to develop flexible electrodes. The high surface area, highly ordered structure, excellent electronic and mechanical properties allowed ACNT to

compete with other CNTs as the choice of electrode materials. ACNT/poly (3,4 thylenedioxythiophene)/PVDF composite layer can show stable capacity of 265mAhg^{-1} at 0.1 mA cm^{-2}, which the capacity is almost 50% higher than a free-standing SWCNT paper (173 mA h g^{-1}), thanks to its highly stable structure and larger surface area. ACNTs can be grown onto flexible grapheme paper by CVD method.[19] In Figure 1.3 (a), a free-standing ACNT/GP film can show stable capacity of 290mA hg^{-1} at 30mAg^{-1}. The fast ion transport paths provide by ACNTs attributes to the relative good performance. However, due to the complex preparation and expensive experimental requirements, this material is less favorable than the others. By using vacuum filtration, a flexible Fe_3O_4/SWCNT electrode was synthesized by embedding FeOOH nanorods in an interconnected SWCNT network through vacuum filtration followed by annealing (Fig.1.3b). With a 5% SWCNTs, this electrode obtains high reversible capacity of 1000 mA h g^{-1} at 1C and a high-rate capability of 600 mA h g^{-1} at 10 C. some other method was also been developed, such as using aerosol spray process to synthesize Fe_3O_4 hybrid spheres that assembled into robust CNT network. CVD self-assembly is another way to build CNT flexible membranes that can avoid using surfactants in vacuum filtration. In this case, a flexible Fe_2O_3/SWCNT electrode material was prepared by Zhou et al. The loading of the active material can reach 88 wt% (Fig. 1.3c). In addition, a dry-drawing method from SACNTs to synthesize SnO_2 /CNTs hybrid sheet was also been reported by Fan's group. As a binder-free anode, it delivered an initial charge capacity of 851 mA h g^{-1} and retained 950 mA h g^{-1} after 50 cycles at 0.1C (Fig. 1.3d).

Other high capacity anode materials such as Si, Ge, Sn and some transition metal oxides have attracted great interest as potential substitutes for carbonaceous materials mostly due to their high capacities. These materials often suffered from huge volume expansion, particle aggregation and unstable structure during cycling. Rigid metallic current collectors cannot restrict the volume

expansion of these materials, in which large internal stress leads to pulverization and delamination that decreased the cycling stability. However, the porous, high surface area structure of the CNTs makes it as a suitable substrate to support these active materials with high capacities. The matrix of the high capacity materials with flexible CNTs was then promising in developing highly flexible electrodes.

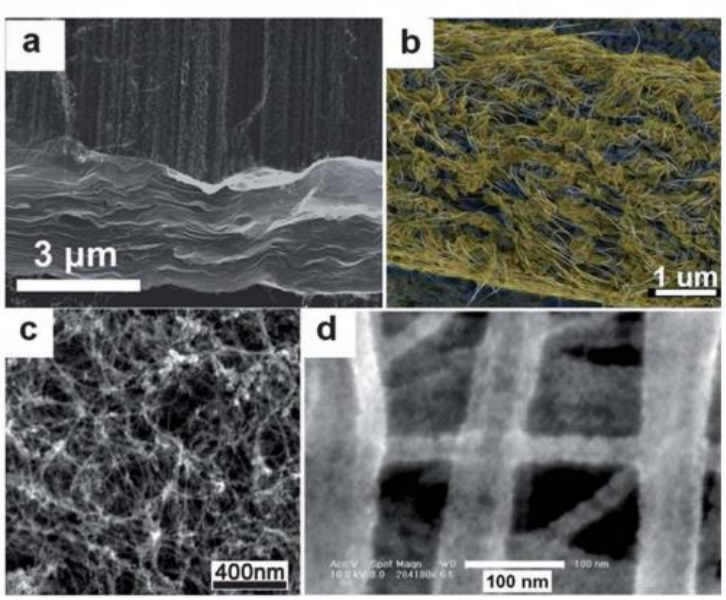

Figure 1.3 (a) Cross-section SEM image of an ACNT/GP film.[20] (b) Cross-section SEM image of a nanostructured Fe_3O_4/SWCNT electrode with colorization for improved contrast.[21] (c)SEM image of a Fe_2O_3/SWCNT membrane.[22] (d) SEM image of a SnO_2/CNT hybrid sheet.[23]

1.2.1.2 CNT-based cathode materials for LIBs

At the cathode side of the LIBs, lightweight and chemically inert CNTs plays a much important role to form an electrode. Since the oxidizing corrosion often occurred on Al current collector under high voltage, a lose contact between active materials and the current collector surface might occur. The lost contact of the active materials with current collector can lead to huge increase in internal resistance.

As described, CNT substrate incorporating with $NaxV_2O_5$ increased the cathode specific

capacity by 20-60% compared to Al foil coated $NaxV_2O_5$.[24] The absence of binder and conductive carbon additives improved cell performance and the lack of Al foil allowed high voltage electrolytes. The anti-oxidative ability of CNTs can provide long-term stability of the cathode structure and hence enable high voltage electrolytes usage which will cause Al foil corrosion. In addition, direct growth of $LiMn_2O_4$ on flexible CNTs was also reported.[25] Through redox reactions between CNTs and $KMnO_4$ with subsequent hydrothermal treatment with LiOH, the resulting cathode showed good reversible capability and cycling stability.

All methods above require high energy consuming equipment and complex synthesis steps, which hindered them from mass production. In one of the recent research projects, a breakthrough was announced. Simple ultrasonication and co-deposition technique were adopted to fabricate flexible electrodes, in which commercial $LiCoO_2$ particles were embedded in the 3D structural network of super-aligned CNT arrays (SACNTs) (Fig. 1.4)[26]. According to this advanced research, the flexible electrodes were comprised of as much as 95 wt% $LiCoO_2$ active material and only consist of 5wt% SACNTs as both conductive additive and structural framework (Fig 1.4b-c). The unique composite showed higher conductivity, strength and Young modulus compared to conventional electrode mixture $LiCoO_2$ and Super P. This typical $LiCoO_2$ /SACNT cathode material obtained high capacity around 151.4 $mAhg^{-1}$ at 0.1C, 142.0 $mAhg^{-1}$ at 1C and 137.4 $mAhg^{-1}$at 2 C (Fig.1.4d). Compared to the existing method with Super P., this work showed a good improvement on its capacity and mechanical strength.

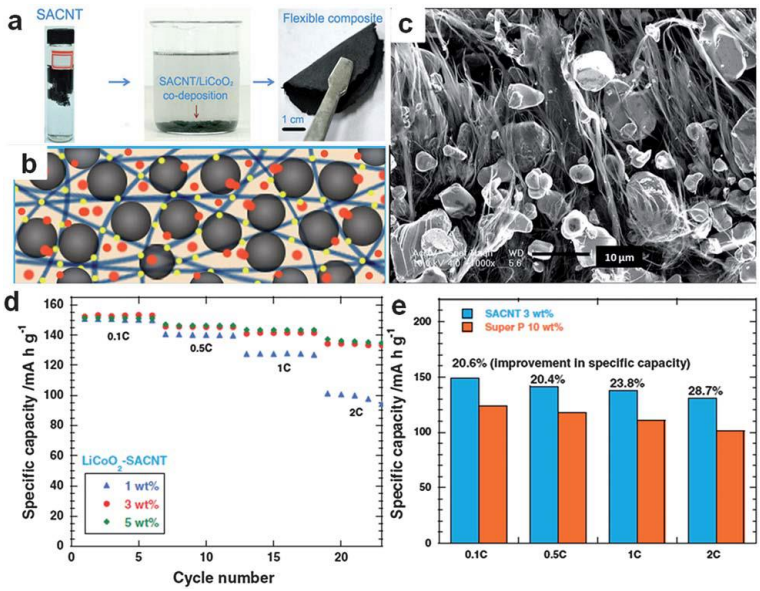

Fig. 1.4 (a) Fabrication of a $LiCoO_2$/SACNT composite. (b) Schematic of the structure of the $LiCoO_2$/SACNT cathode. (c) Cross-sectional SEM image of the $LiCoO_2$/1 wt% SACNT composite. (d) Rate performance of the $LiCoO_2$/SACNT cathode. (e) Specific capacities of the $LiCoO_2$/3 wt% SACNT cathode and the classical $LiCoO_2$-10 wt% Super P cathode at different rates, based on the total mass of the cathodes.[26]

1.2.1.3 CNT-based current collector for LIBs

Due to the superior properties of CNTs, the research of its application does not stop on electrode materials. As one of the most important components of the batteries, current collectors and separators can also benefit from CNTs. In Cui group's recent work, other than mixing CNTs homogeneously with active materials, a CNT-based current collector was fabricated to laminate with active material layers (Fig. 1.5a-b). In this work, a lightweight CNT current collector accompanies with LCO and LTO coating as cathode and anode materials, respectively, was able to light up a LED device. The material's good mechanical flexibility allows bending 50 times down to a radius <6mm without failure. The energy density of the flexible LIB is about 108 mW h g-1, and its total energy for the cell can be increased by simply stacking multiple cells in parallel (Fig 1.5d) and the assembled battery can light up LED device as Figure 1.5 (c) shows.

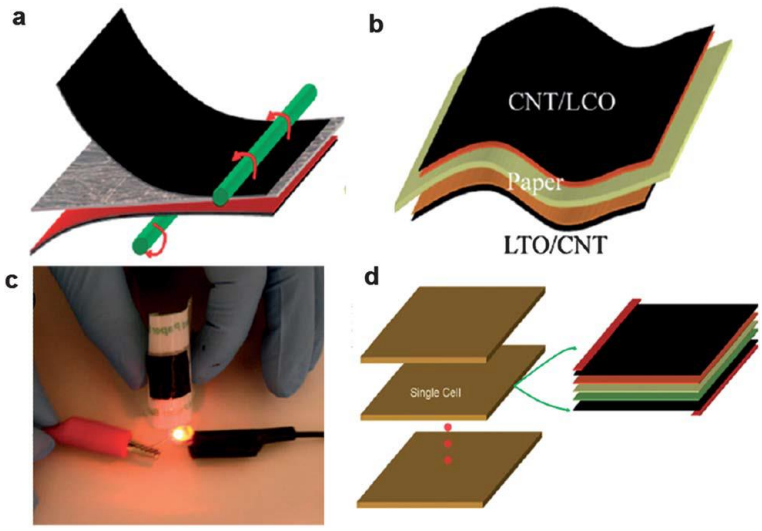

Fig. 1.5 (a) Schematic of the lamination process. A freestanding film is laminated on paper with a rod and a thin layer of wet PVDF. (b) Schematic of the paper LIB structure. (c) Flexible Li-ion paper battery lights an LED device. (d) Schematic of stacked cells separated by a 10 mm thick paper. [27]

In summary, there are four main advantages of using CNT network in constructing high performance flexible electrode materials:

(1) The network of the CNTs provides resilient and strong base which can stabilize electrode structure during cycling process.

(2) Fast electron transport paths are enabled which also improves electrochemical reaction kinetics of the electrode.

(3) The special network structure provides channels for efficient ion transport.

(4)A flexible and robust CNT network gives the electrodes structural integrity and accommodates repeated mechanical deformation in flexible LIBs, leading to better cycling stability, rate capability and mechanical durability

1.2.2 Graphene-based electrodes for flexible LIBs.

Graphene is another promising material in the electrochemical energy storage field since its high surface area (2630 m^2 g^{-1}), lightweight, wide potential windows, high conductivity (2.5×105 $cm2V^{-1}$ s^{-1}) and superior mechanical flexibility (a Young's modulus of 1 TPa and intrinsic strength of 130 GPa). In recent years, the development of large scale and low-cost production has further strengthened the important role of graphene and its hybrids in energy storage. Compared to CNTs, graphene shows unique characteristics. For instance, the theoretical surface area of graphene is higher than that of DWCNTs and MWCNTs. The large surface area provides more electrochemical reaction active sites in energy storage.

In addition, graphene surpasses CNTs on cleaning the residual metallic impurities, which is difficult to be removed from the porous structure and thus affects the cell performance.

1.2.2.1 graphene-based anode materials for LIBs

Graphene-based papers were first investigated as flexible electrode materials by Wallace's group. It can be easily synthesized through flow-directed assembly by vacuum filtration.[28] Although the graphene paper used was mechanically strong with a Young's modulus of 41.8 GPa and a tensile strength of 293.3 MPa and showed a high electrical conductivity of 351 S cm, it displayed significant drop (only 84 mA h g^{-1}) at the second cycle with a large irreversible capacity, most likely due to the restacking of the graphene sheets.[29] An unannealed lightweight graphene paper was also used as a binder-free anode, which was prepared by hydrazine reduction of a graphene oxide paper, although the cycling stability is improved, the capacity and rate capability

cannot be satisfied. Generally, graphene sheets are prone to agglomerate during the reduction and drying process because of strong inter-planar pi–pi stacking and Van Der Waals interactions between graphene, and tightly compacted graphene sheets can greatly inhibit efficient electrolyte diffusion.

To prevent the restacking of graphene, CNTs can be used as the support, which randomly disperse between the graphene sheets to allow more effective contact between electrolyte and graphene. In order to increase the cross-plane diffusivity, in-plane porosity was introduced into the graphene sheets in the graphene paper by ultrasonic vibration and mild acid oxidation.[30] These pores facilitate ion transport and storage, improving the power capability of the graphene electrodes, especially at high rates.[31]

In addition to the commonly used vacuum filtration method to fabricate flexible graphene paper, Liu et al. developed an approach to fabricate graphene paper with a wrinkled structure by mechanically pressing a graphene aerogel.[32] This free-standing graphene paper is highly flexible and shows high charge capacity of 864 mA h g^{-1} with a Coulombic efficiency of above 98% from the second cycle, high rate capability and good cycle performance after 100 cycles.

1.2.2.2 Graphene-based cathode materials for LIBs

As the bottleneck of producing high performance flexible LIBs, cathodes materials have been intensively researched. According to the recent research, Iron trifluoride (FeF_3) can act as conversion reaction cathode material for high theoretical capacity and redox potential. By synthesizing FeF_3/graphene paper with electrostatic assembly, the hybrid paper cathode with uniformly dispersed FeF_3 NPs and opening porous channels, shows a relative high capacity (580mAhg at 100mAg) and good cycling performance.[30, 33]

Another promising cathode material that has low cost, high specific capacity and relative abundance resource in nature is V_2O_5.[34] In recent years, V_2O_5 NWs has been researched to be incorporated with graphene to form free-standing paper due to its superior flexibility and robust structure. With a 15 wt% V_2O_5 NWs, it can produce a specific capacity of 94.4 mAh g^{-1} which can be preserved over 100,000 cycles at high current density (2-3 orders of magnitude longer than regular cathode materials). In Figure1.6, a graphene-based flexible LIB was fabricated using flexible graphene paper and V_2O_5/graphene paper as anode and cathode, respectively. Through pulsed laser deposition technique, V_2O_5/graphene paper was produced and possessed both good mechanical strength and electronic conductivity.[35]

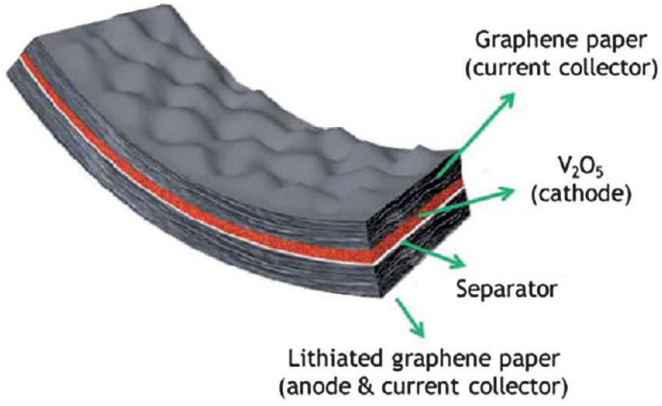

Figure 1.6 Schematic of the flexible Li battery based on the graphene papers. [35]

1.2.2.3 Graphene-based 3D macrostructure as current collector materials for LIBs

Recently, a 3D highly conductive graphene macrostructure, so called graphene foam (GF), was synthesized using Ni foam template-directed CVD.[36] Due to its interconnected graphene network, this material was able to provide high electrical conductivity and mechanical strength. Based on

this technique, Li et al. developed 3D interconnected conductive ultra-thin graphite foam (UGF) as free-standing and lightweight current collector to reduce the weight and resistance of the electrodes.[37] LiFePO4 was drop-casted onto the UGF to produce a cathode material and presented excellent electrochemical stability. Li et al. continued on this work, using 3D GF to drop-cast $Li_4Ti_5O_{12}$ and $LiFeO_4$ as anode and cathode, respectively. Without using any metal current collectors, the hybrid electrodes obtained excellent electrical conductivity and pore structure that allowed rapid electron and ion transport. The hybrid electrode materials were able to be repeatedly bended to a radius of <5mm without structural failure and loss of performance (Fig. 1.7 a-d), giving great promise in future flexible electronics development.[38]

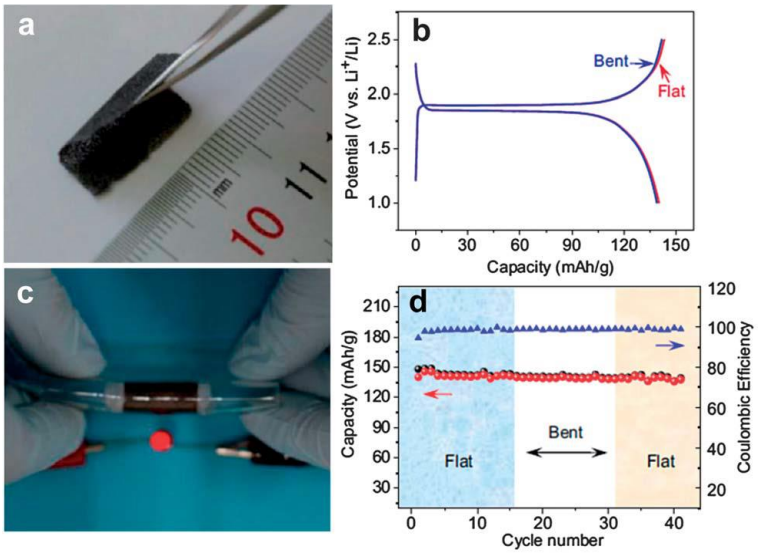

Figure 1.7 (a) Photograph of a free-standing flexible Li4Ti5O12/GF being bent. (b) Galvanostatic charge–discharge curves of the battery when flat and when bent. (c) Lighting a red LED device under bending. (d) Cyclic performance of the battery under flat and bent states.[38]

Graphene-based flexible hybrids exhibit exciting properties which exceed the intrinsic properties of each component and introduce some new properties and functions. The superiority of graphene-based flexible electrode can be ascribed to the fact that:

(1) The flexible and strong graphene lays a foundation for constructing graphene-based high-

performance flexible electrodes;

(2) The graphene restrains the volume expansion during lithium insertion/extraction;

(3) The pores developed between a secondary phase and graphene facilitate fast ion transport;

(4) The interconnected graphene framework suppresses particle aggregation, while the active materials suppress the agglomeration/re-stacking of the graphene sheets and increase the available surface area;

(5) The electrically conducting graphene network ensures good electrical conductivity of the electrodes.

1.2.3 Carbon cloth-based electrodes for flexible LIBs.

Other than CNTs and Graphene- based flexible electrodes, carbon cloth obtained high flexibility and strength that is capable of being a flexible LIB electrode material as well. Carbon cloth can serve as good conductive support for high performance electroactive materials such as $ZnCo_2O_4$ NW arrays or $Ca_2Ge_7O_{16}$ NW arrays. For example, $ZnCo_2O_4$ NW arrays anode material can be grown on the carbon cloth using hydrothermal method. It exhibits a 99% capacity retention after 160 cycles at 200mAg-1 and retains 605 mAhg-1 at 4500 mAg-1. The intimate contact of $ZnCo_2O_4$ NW arrays and carbon cloth with good charge transfer, the loose and open NW arrays with large accessible area and the fast Li+ ion diffusion paths and buffer space enable the high performance (Fig. 1.8 a). A prototype flexible battery consisting of $ZnCo_2O_4$/carbon cloth anode and $LiCoO_2$/Al foil as anode and cathode respectively was built in Figure 1.8 (b). Although its loading density of active material is relatively low, the concept of this carbon cloth-based flexible battery has been proven and used as power source in devices such as LED and LCD (liquid crystal displays). [39]

CNT non-woven fabric can also serve as flexible substrate for coating Si to create high capacity

flexible anode with high mechanical strength, reported by Evanoff et al. In their work, Si-CNT fabric was able to reach stable capacity around 500 $mAhg^{-1}$ over 150 cycles with 90% of its original strength by preventing Si pulverization through limiting the amount of Lithium ions insertion.[40]

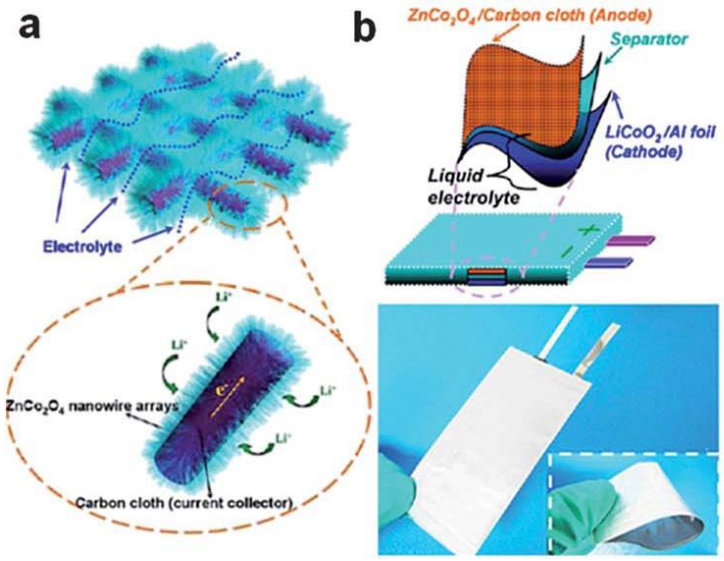

Figure 1.8 (a) Schematic of a ZnCo2O4 NW array/carbon cloth electrode. (b) Illustration of the fabrication of a hierarchical 3D ZnCo2O4 NW array/carbon cloth/liquid electrolyte/LiCoO2 flexible LIB.[40]

A general strategy was also developed in order to fabricate flexible lithium metal oxides such as $LiMn_2O_4$ with carbon textile composites by in situ growth and chemical lithiation (figure 1.9).[41] Carbon textiles acts as lightweight flexible current collector in this case and promotes charge transfer and ion diffusion, which ultimately improves the overall energy density of the battery. For instance, taking $Li_4Ti_5O_{12}$/carbon textile as anode and $LiMn_2O_4$/carbon textile composite as cathode, the battery shows good rate capacity of 103 $mAhg^{-1}$ at 90 C and obtains only 5.3% of capacity loss after 200 cycles at 10 C. The combination of these two can be expected to use on wearable electronic devices.

Figure 1.9 Schematic of the fabrication of lithium metal oxide/carbon textile composites. [41]

Carbon cloth is a kind of commercially available material with low cost, high flexibility and light weight. Creating electrode material using carbon cloth without binders and additives is viable. Its structural advantage allows it to act as a great platform for constructing flexible batteries. Both direct growth and deposition/coating methods were recognized as efficient route to create better transport of electrons and ions. The advantages of carbon cloth can be summarized as:

(1) Tight adhesion of the active material on carbon cloth provides good conductivity and stability during the cycling.

(2) Porous structure allows easy diffusion of lithium ions into the material.

(3) The flexible substrate allows for accommodation of volume expansion during lithium insertion and extraction.

1.3 Electrolyte materials for flexible LIBs.

Electrolyte with high ionic conductivity and chemical compatibility with electrodes is a key component for building a Li-ion battery. However, commercial Li-ion batteries have disadvantages such as toxicity, flammability, volatility, and potential leakage danger which hindered its application being use in FLIBs.[42] Therefore, to solve the problem, gel electrolytes and solid-state electrolytes were being focused.

For a FLIB, with the repeated deformation of batteries, stable interface contact between the electrode and electrolyte is of critical importance. Fluidic properties of liquid electrolytes restrict stringently the design and size of a flexible battery. With the increase of the energy density of LIBs, safety problems have become a significant concern in their practical use.[16] Solid-state and gel electrolyte are safer and more reliable compared with liquid electrolyte. Solid-state electrolytes are highly stable, allowing a wide range of operation temperatures and exhibiting negligible self-discharge. However, they can suffer from low ionic conductivity ($\sim 10^{-6}$ S cm^{-1}) at room temperature and their lack of fluidity can results in poor interfacial contact. Polymer electrolytes, composed of conventional liquid electrolytes within polymer matrix, have both high ionic conductivities and good mechanical flexibility. Polymer electrolyte can be flexible and maintain stable contact with the electrodes even though with repeated bending and stretching. Therefore, at present, polymer electrolyte will be one of the best choices for flexible LIBs.

The alternative polymer-based electrolytes for LIBs must obtain good ionic conductivity, good thermal, chemical and mechanical stability, relatively high lithium transport number and compatibility with their electrodes. Many of the polymer electrolytes such as Polyethylene oxide (PEO), polypropyleneoxide (PPO), polyvinylidene fluoride (PVDF), polyacrylonitrile (PAN) and polymethyl-methacrylate (PMMA), were selected because of their good performance.[43] However, within large group of the electrolytes, PEO and PVDF-based matrices are currently the best choice to prepare SPEs and GPEs, respectively.

Solid polymer electrolytes (SPEs) are ion-conducting single-phase or composite systems based on polymer-salt complexes. They can be synthesized by solvent casting, hot pressing, lamination, extrusion and in situ polymerization. As suitable matrixes for SPEs, polyethylene oxide and its copolymers have been tested for many years (different PEOn-LiX systems). The ion conduction is

based on an oxygen-assisted doping mechanism that takes place in polymer amorphous phase. Due to the semi-crystalline nature of the polymer, its conductivity shows relatively low value at room temperature but abruptly increases above the melting temperature, reaching 1mS cm^{-1} at 80-90 ℃, where most polymer is in a viscous liquid state. Its anion mobility along the polymer chains normally performs better than cation. Low lithium transport numbers (t^+ <0.3) are also obtained, which may be improved by choosing salts with larger organic anions and huge electron delocalization. The presence of the salt increases the polymer amorphous fraction. At higher salt contents, the crystalline aggregates can lead to reduction of the conductivity and transport numbers, because of the formation of ion pairs and phase segregation. However, there are some 6:1 crystalline complex such as PEO_6-$LiAsF_6$ may offer unique cylindrical structures where lithium ions reside without being coordinated by anions (Fig.1.10). [44]

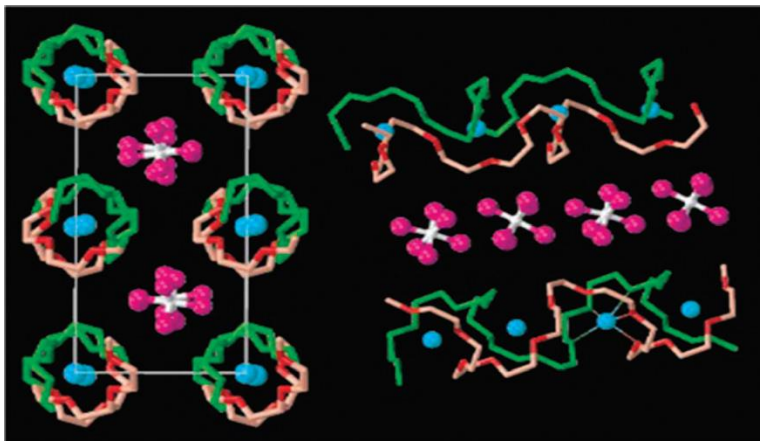

Fig. 1.10 The structure of PEO_6–$LiAsF_6$ (hydrogen atoms are not shown). Left: view of the structure along the axis, showing rows of Li^+ ions perpendicular to the page. Blue spheres, lithium; white spheres, arsenic; magenta, fluorine; green, carbon and oxygen in chain1; pink, carbon in chain 2; red, oxygen in chain 2. Right: view of the structure showing the relative positions of the chains and their conformations. Thin lines indicate coordination around the Li^+ cation.[44]

The technology using PEO-salt SPEs requires acceptable compromise among following features: 1) suitable ionic conductivity; 2) good mechanical properties; 3) high transport number. Many efforts were made to this aim. One way was PEO blending and/or cross-linking with other

compatible polymers such as polyacrylic acid (PAA), polymethylmethacrylate (PMMA), which increase the conductivity and lithium transport number by blocking the anion.

Dispersion of ceramic phases (filters) in PEO-based electrolytes to form nanocomposite systems is currently the most effective way to improve thermal, chemical and mechanical stability. The improvement is mainly due to suppression of the PEO crystalline fraction.

Polymer alternative to PEO to fabricate the solid polymer electrolytes were developed during the last decade. All these matrix contain ethylene oxide units such as polyethylene glycol (PEG), polyethyleneoxide-methylether methacrylate (PEOMA), and so on. [43]

Gel polymer electrolytes (GPEs) are formed by swelling polymer matric with electrolyte solution that containing high-boiling solvents and/or plasticizers. It is also known as the hybrid polymer electrolytes (HPEs). Gel-polymer electrolytes are one of the most commonly used solid electrolytes in flexible batteries. GPEs simply composed of a polymer matric filled with liquid electrolyte and possessed both cohesive properties of solids and the diffusive properties of liquids, which lead to high ionic conductivities and good mechanical flexibility. Many of the polymer matrix were tested in the past, such as PAN PMMA, PVC and even PEO.[43, 45, 46] The most important matrix in this electrolyte is (PVDF-HFP), which is available with HFP molar contents in the range of 5–25%. These materials were firstly proposed as electrolytes for LIBs by Bellcore.[47] Up till now, they are the most commonly used in the LPB market.

GPEs are multiphase systems where crystalline, amorphous/swollen and liquid zones coexist. The polymer host becomes more amorphous in swollen state and its glass transition temperature, Tg, which is generally sub-ambient, further decreases by increasing the liquid content. Contrary to SPEs, ions move in liquid or liquid-like phases in this system, obtaining good conductivity values.

The simplest way to fabricate the flexible LIBs with GPEs is to sandwich a GPE sheet between the electrodes. The electrodes were precoated with GPE by dipping. And then additional 100 μm-thick GPE layer was sandwiched between electrodes. Room temperature operation of the battery is acceptable. Saunier et al. made a flexible LIB using poly (vinylidene fluoride) [PVDF]-based GPE membrane with a $LiCoO_2$/Al foil cathode and carbon anode that were hot-pressed together.[48] Its energy density was able to reach 95 W h kg^{-1}. Appetecchi et al. also demonstrated a flexible LIB by laminating a graphite anode and a chromium-doped lithium manganese oxide spinel cathode with a GPE membrane composed of a mixture of $LiClO_4$–EC–diethyl carbonate (DEC)–PAN. The electrolyte had high ionic conductivity (4×10^{-3} S cm^{-1}) at room temperature, enabling a comparable electrochemical property to that observed in conventional liquid electrolytes. [49]

1.4 New structure and stretchable lithium ion batteries

In order to fabricate flexible LIBs, individual cell components with different mechanical properties are assembled together. Therefore, during deformation of the device, strain arises not only in each component, but also at the interfaces between components. The strain in the device under flexure or distortion must be managed. Therefore, the packaging materials and batteries' structure design are very important for the mechanical performance.

1.4.1 cable/wire type flexible LIBs

With the rapid development of different electrode materials for flexible LIBs, the structure of

the LIBs has also started to reform. During recent research, flexible cable/wire structured LIBs started to gain attraction and show their future potentials. A cable/wire design of the LIBs has provided a new concept of the battery design that enabled better flexibility and devices design innovation.[50, 51] In Figure 1.11(a-b), Kwon et al. has developed a novel cable-type LIB that can be place anywhere in different shapes with its perfect flexibility. This cell is constructed by hollow spiral Ni-Sn anode with $LiCoO_2$ cathode and multi-helix structured polyethylene terephthalate nonwoven separator.[51] The cable shows excellent mechanical flexibility and strength under severe bending and twisting (Fig. 1.11 c-d).

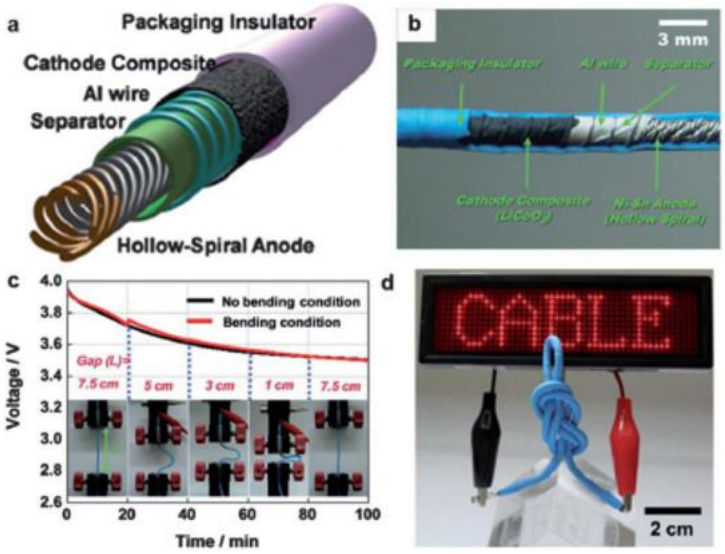

Fig. 1.11 (a) Schematic of the cable cell with a hollow-helix anode. (b) Photograph showing the side view of a cable cell separated into component layers. (c) Discharge characteristics with changes in bending strain every 20 min. The discharge rate was 0.1 C and the grip speed of the testing machine was 100 mm min^{-1}. (d) Photograph of a highly flexible cable cell under twisting. [52]

1.4.2 Transparent flexible LIBs[53-56]

In recent years, some of the new application designs open a new requirement for transparent/

semi-transparent flexible batteries. This requires all components including electrode, current collectors, electrolyte, separators and packaging to be transparent. As the most promising material, tin-doped indium oxide (ITO) has occupied the market with its transparency and relatively good flexibility. However, the low abundance of indium, significant electrical conductivity drops, low columbic efficiency and poor cycling performance still hindered the use of ITO in transparent LIBs. Yang et al. introduced a micro fluidics-assisted method that pattern graid-like transparent cathode ($LiMn_2O_4$)/anode ($Li_4Ti_5O_{12}$) on a flexible polydimethylsiloxane (PDMS) substrate. Combine with PVC and transparent electrolyte, this transparent battery can light up a $10WhL^{-1}$ LED (Fig. 1.12).[57]

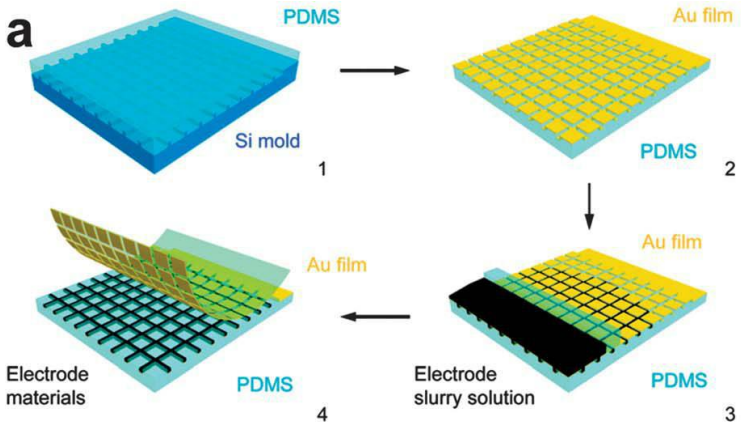

Fig. 1.12 (a) Process for the synthesis of a transparent battery: (1) transfer a grid pattern from a silicon mold to PDMS; (2) evaporate a gold current collector on the PDMS substrate; (3) fill in battery electrode materials by a microfluidics-assisted method; and (4) peel the gold film from the top of the PDMS substrate. [57]

1.4.3 Stretchable flexible LIBs

Stretchable LIBs are another new development that attracts lots of attention nowadays. Many of the special electronic devices such as skin sensors not only requires power source that can bend, but also requires mechanical stretch ability to a certain degree while the device remains its function. In this case, CNTs and conductive nanowire-assembled net-shape structures are commonly used.

Some “wavy” layout, stretch-tolerant structures that electrode are coated on pre-strained PDMS substrate are used as new structural design choice as well.[58, 59]

According to Rogers’s group in their recent work, stretchable battery was developed by using segmented design with deformable electrical interconnects in self-similar geometries. Using $LiCoO_2$ and $Li_4Ti_5O_{12}$ as cathode and anode respectively, silicone elastomer as substrate, with gel electrolyte, this battery is useful for many practical applications such as in skin-mounted systems that are susceptible to physical contact. The potential to spread the battery system over arbitrary curve surface became very important for flexible/wearable devices development (Fig.1.13 a-c). [60] Based on the elaborate design scheme, the batteries demonstrate biaxial stretch ability with strains up to 300% (Fig. 1.13d), an area capacity density of 1.1 mA h cm^{-2} at a charge–discharge rate of 0.5 C and can be folded (Fig. 1.13e), twisted (Fig. 1.13f) or mounted on human skin (Fig. 1.13g) to light a LED without noticeable dimming.[61]

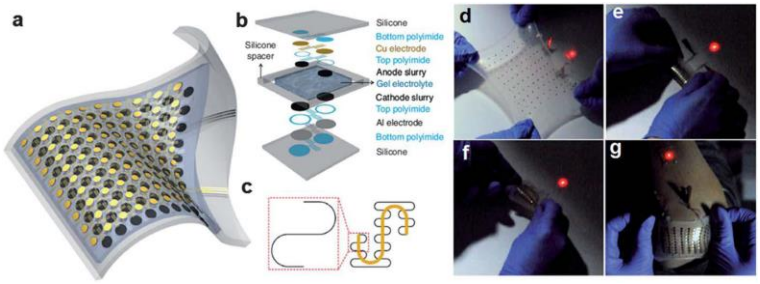

Fig. 1.13 (a) Schematic of a complete device in a state of stretching and bending. (b) Exploded layout of various layers in the battery structure. (c) Illustration of ‘self-similar’ serpentine geometries used for the interconnects. (d–g) Operation of a battery connected to a red LED while (d) biaxially stretched to 300%, (e) folded, (f) twisted and (g) mounted on the human elbow. [61]

In spite of the achievements of flexible LIBs, there exists substantial room for the development of high-performance flexible energy storage devices. Some challenges still need to be solved to forward the application of flexible LIBs.

(1) To fabricate highly flexible energy storage devices with high energy/power densities,

operational safety and excellent cyclic stability are still great challenges.

(2) The electrolyte plays a key role in securing battery safety. All solid-state flexible lithium batteries are thus promising because it gets rid of combustible organic electrolytes.

(3) Lightweight, thin, flexible and stable packaging materials with exceptional barrier properties are also needed to protect battery from being affected by the external environment and ensure good mechanical performance.

(4) The assessment criterion of flexibility, such as electrochemical performance with respect to the bending radii of device or bending times, needs to be standardized.

Chapter 2 The objective and scope of this dissertation

A comprehensive literature research shows the key progress in the development of FLIBs and their key challenges. Many innovations of cell structures and incorporation of active materials have been uncovered for FLIBs. However, from the material perspective, the lack of intrinsically flexible active materials and fabrication methods substantially hampers the progresses in seeking high electrical performance and mechanical strength of the FLIBs. To incorporate with the FLIBs, electrolytes is also under challenges concerning their safety issue with organic solvents or their poor ion transportation in SSEs.

In this dissertation, to integrate above requirements into FLIBs, robust structure design of cathode materials was developed and demonstrated with experiments. At the same time, new strategies on FLIBs electrolyte has also been develop with superior electrochemical performance. Specifically, a combined exploration of material and structural design can be separate into two main categories: (a) development of novel structure electrode materials V_2O_5/CNT with facile

fabrication method; (b) facilitates ion transportation in GPEs with MOFs additives.

Compare with the poor mechanical strength of conventional electrode materials and sluggish ion transportation in most of the GPEs, these methods not only provide structural design of the active materials regarding robust mechanical strength, but also possesses high battery safety while maintaining high electrochemical performance. The above-mentioned findings are expected to further push the actual commercialization of the FLIBs.

Chapter 3 Flexible Electrode material based on V_2O_5-CNT nanowire composite.

It has been investigated that one-dimensional materials, such as nanobelt, nanowire/fiber and nanotube are able to provide transport and conductive merits because of the short diffusion distance in the radius direction and long electronic conductive pathway in axis direction. Therefore, by forming network architecture, an even higher conductivity can be achieved without much loss of surface properties.

By taking full advantage of this concept, we herein report a facile and cost-effective method, which intergraded the *in situ* generated polytetrafluoroethylene (PTFE) fibrils, for the synthesis of V_2O_5-CNT nanowires matrix with superior mechanical strength. The composite was used as active material to assembly within lithium-ion batteries, exhibiting Young's modulus at 800 MPa and 103.1×10^{4} J m^{-3} toughness while capacity retention maintained more than 86% after 1000 times bending at 1C.

3.1 Introduction

Lithium-ion batteries (LIBs) are currently served as the major consumer market power banks due to their high specific energy and long lifespan. As mentioned above, there are many cathode active materials been developed and utilized into applications ($LiCoO_2$, $LiMn_2O_4$ and $LiFePO_4$). However, searching for higher power and higher energy density within lithium ion batteries is endless. In recent years, due to rapid blooming of flexible electronic devices, new electrochemical systems are required to reduce their size to further incorporate with the appliance. As a result, flexible electrodes were studied extensively to realize flexible electronic devices. In order to fulfill this, a cathode with both high energy density and high mechanical strength is urgently needed.

As one of the most abundant elements in earth's crust，vanadium is a common transition metal and has four oxidation states of V^{2+}, V^{3+}, V^{4+} and V^{5+}, which associated with VO, V_2O_3, VO_2 and V_2O_5, respectively.[62] Vanadium pentoxide (V_2O_5), as a typical intercalation compound exhibits a well-ordered orthorhombic crystalline structure, holds large theoretical capacity of 294mAh/g^{-1} when storing two lithium ions. Compared with the commercialized cathode materials in Table 3-1, V_2O_5 maintains higher practical capacity（170 $Whkg^{-1}$）because of multi-electrons storage mechanism. In addition, while synthesized, its one-dimensional structures such as nanowires, nanorods, and nanotubes, contains huge potential to form flexible electrodes matrix while incorporated with other binders or composites.

Table 3-1. Capacities and energy density comparison of typical LIBs cathode[63]

Active materials	Cell voltage (V vs. Li^+/Li)	Theoretical specific capacity（mAh g^{-1}）	Practical capacity（mAh g^{-1}）	Theoretical specific energy (Wh kg^{-1})	Practical specific energy (Wh kg^{-1})
$LiCoO_2$	3.9	274	140	584	100-150
$LiMn_2O_4$	4.1	148	110-120	424	80-100
$LiFePO_4$	3.4	170	160	510	80-100
$Li_xV_2O_5$	2.5	294	250	735	120-170

However, the practical application of V_2O_5 still seriously hindered by slow lithium-ion diffusion and low electronic conductivity, which leads to poor cycling stability and poor rate capability in LIBs. To overcome these barriers and further improve the mechanical performance, different forms of V_2O_5 incorporating with carbon nanotubes, graphene sheets, and carbon cloth sheets were reported. Dewangan et al. synthesized V_2O_5 nanofiber-bundles by a hydrothermal method using a vanadium hydroxylamido complex as a vanadium precursor.[64] O'Dwyer et al. synthesized VO_x nanotubes through a surfactant-assisted templating method.[65] Xilai Jia et al. synthesized mesoporous V_2O_5 and penetrating CNTs via an aerosol-spray drying process.[66] Bo Yan et al. proposed reduced graphene oxide-based functional materials by encapsulated hollow V_2O_5 nano/microsphere.[67] The introduction of carbon materials in metal oxide electrode could effectively improve its conductivity, which has significant enhancement in electrochemical performance.

Notably, among all different carbon-based materials, CNTs were able to form intertwined network with small amount of loading to provide relative strong mechanical support while remain most of their electronical performance. Given V_2O_5/CNT composite as example, the interpenetrating network forming between V_2O_5 and CNT was able to raise the composite electrode stress to 4.8 MPa, which is eight times of LCO/SACNT flexible electrode composite.[68, 69]

Therefore, by taking full advantage of the crosslinking V_2O_5 /CNTs intertwined composite, we further improve it via *in situ* generated PTFE fibrils into existing network structure.

Polytetrafluoroethylene (PTFE), which developed by DuPont, has linear macromolecule structure that can be form into chain conformation. Because its highly symmetric structure with "C-F" bonding on side chain, PTFE appears with high nonpolar and chemical resistance properties. In addition, PTFE also obtains excellent thermal resistance under both low and high temperature (- 190℃ ~ 260 ℃) which allows for numerous applications, especially under harsh environment.[70]

Traditionally, PTFE can be obtained via polymerization of tetrafluoroethylene (TFE). This reaction usually contains radical initiator (ammonium persulfate), with condition of 310-350K and 10-20atm. Fabrication of PTFE is often considered difficult because of the toxicity of TFE and requirement of high-pressure condition. To ease the fabrication method and apply PTFE into electrode, Kazuya Hiratsuka et al. filed a patent using 10% PTFE powder with simple physical kneading method.[71] In this case, PTFE fibrils were synthesized simply by applying small amount of shear force. The fabricated PTFE fibrils perform as the binder for active materials while providing good mechanical support.

Herein, in this work, we had developed a facile and cost-effective way to facilitate both lithium ion transportation and electron transfer speed while maintaining a relatively high mechanical strength via incorporating *In-situ* fibrillated PTFE with interpenetrating V_2O_5 /CNTs network. Our composite matrix achieved Young's modulus at 800 MPa and toughness at 103.1×10^{4} J m^{-3} while a bendable battery shows a capacity of 300 mA h g^{-1} at 0.25 C. Capacity retention maintained more than 86% after 1000 times bending at 1C.

3.2 results and discussions

In-situ growth of the V_2O_5 nanowires within CNT networks led to a highly flexible, dark-green nanocomposites. To study the structure of the composites, we firstly analysis the structure and morphology of the CNTs and V_2O_5 nanowires.

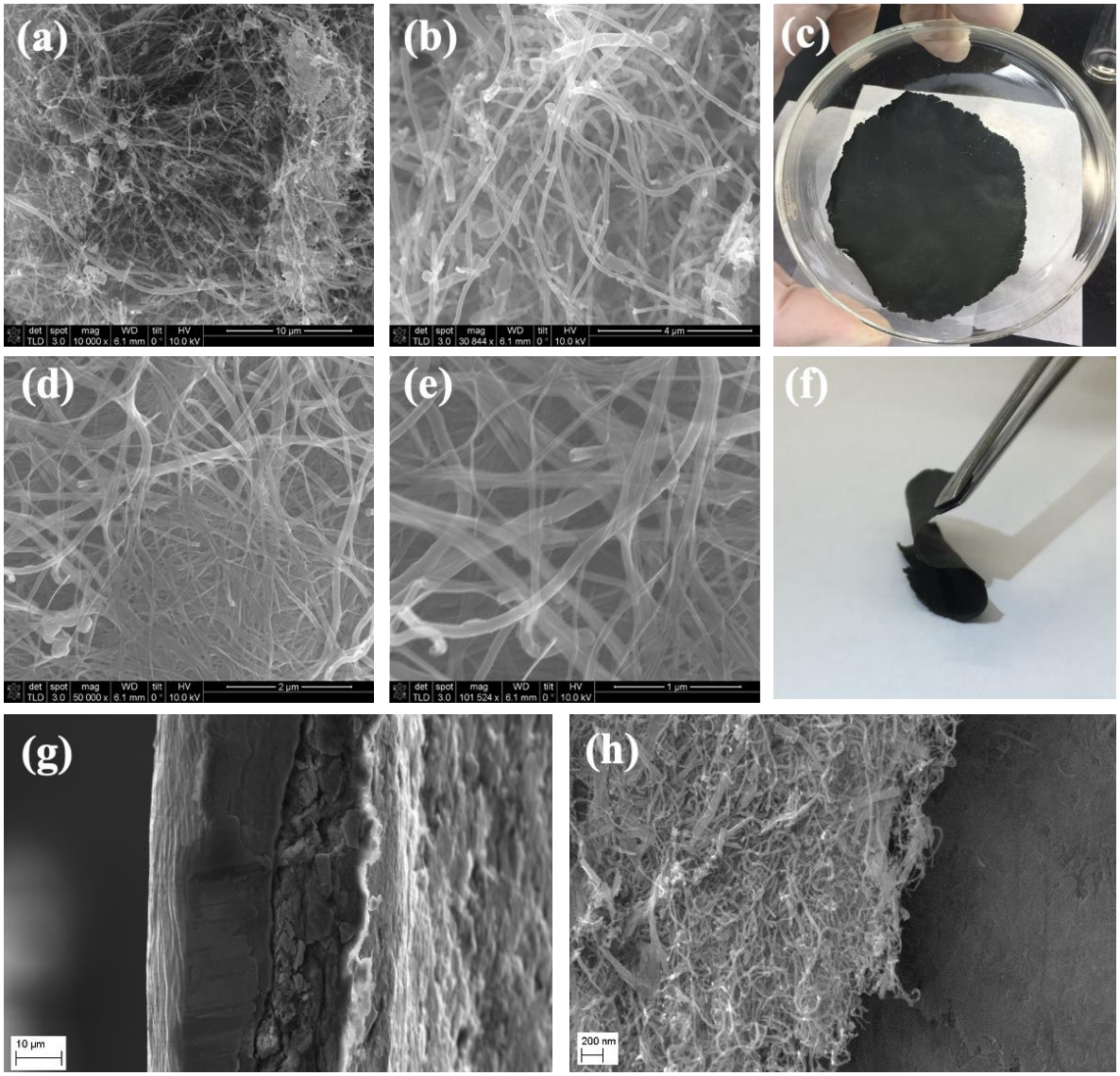

Figure 3.2 SEM image of the V_2O_5/CNTs composites

Figure 3.2 shows representative SEM image of the composites. Within the porous network, the entangled CNTs has a diameter of 10-30nm and lengths around micrometers; The diameter of V_2O_5 nanowires is around 20-50 nm and lengths up to tens of micrometers. The images also revealed the interpenetrating network structures of the nanowires. Such interpenetrating network structure creates intimate contact of the CNT and nanowire networks, enabled rapid electron transport along the trends of the nanowires.

The morphology and structure of the V_2O_5/CNT blended with PTFE were further revealed by Figure 3.2 (g)(h). After hot-press process, PTFE fibrils were infused into the composite framework and attached to the current collector. Fibrils were pulled out from original PTFE particle and reformed into smaller fibrils that connects each other to provide a robust support.

In such hierarchical structure, in-situ growth of nanowires within the CNT network results interpenetrating network structure. X-ray diffraction (XRD) reveals that V_2O_5 nanowires are highly crystalline with well-defined *(001)* reflections at 2-theta degree of 11.1, 15.5, 27.5, 41.5 and 44.5, consistent well with previous studies (Fig. 3.3).

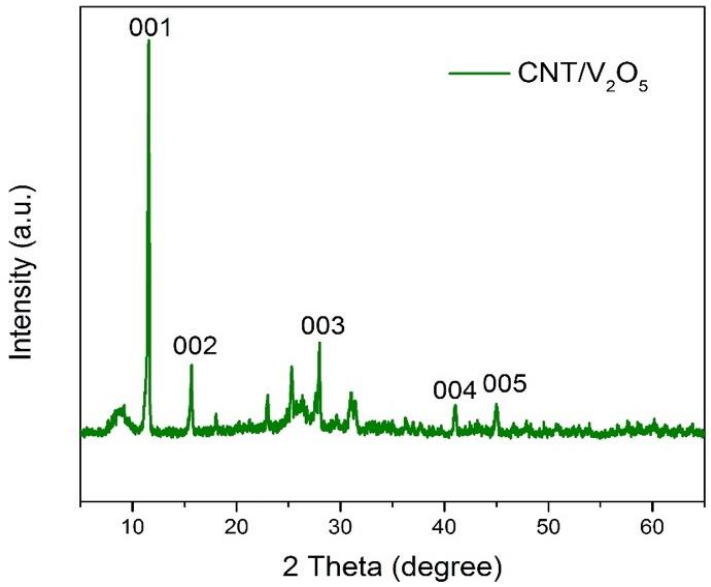

Figure 3.3 XRD patterns of carbon nanotube/vanadium oxide composites

In order to confirm the excellent flexible performance, mechanical tests were conducted on INSTRON 5564 at 2.0 mm/min (Figure 3.4). The stress of the cross-linked electrode of Jia's work is ~4.8 MPa, and modulus approaches ~500 Mpa. Our cathode material shows a stress around 11.2MPa, and modulus is around ~ 800 MPa (Figure 3.4 a). The toughness is increased from 18.2×10^4 J m^{-3} before hot press to 103.1×10^4 J m^{-3} after hot press. The huge improve of stress and toughness suggest that blending of PTFE into the cathode material can further strengthen the network and improve the mechanical performance.

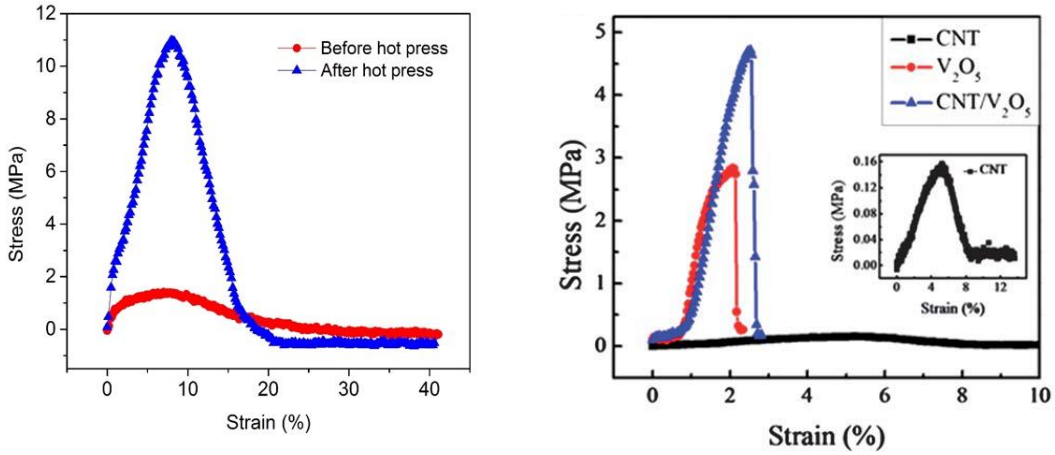

Figure 3.4 mechanical strength comparison between current work and crosslinking approach from Jia, *et al*.

The electrochemical performance of CNTs/V_2O_5 was tested by galvanostatic charge/discharge process using half-cell. In Figure 3.5 (a), the discharge capacity in the first cycle is ~300mAh g^{-1} based on the total mass of the composite electrode. This result indicates that V_2O_5 has two electrons storage process. Note that, after performing the first charge/discharge test, same pouch cell was put onto hand bending test, both working voltage and the galvanostatic profile remained no change in flat and bent state. (Figure 3.5b-d).

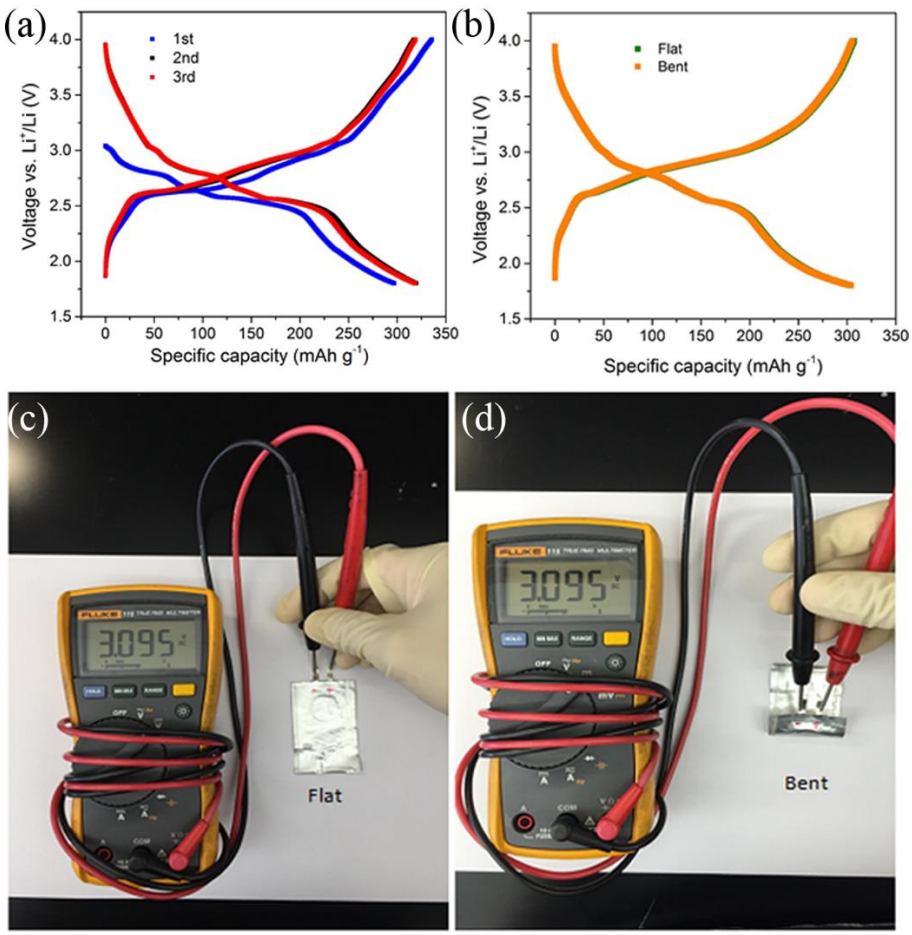

Figure 3.5 (a) First three charge/discharge cycles of a CNT/V_2O_5 composite electrode (25wt% CNTs). The battery was tested at 0.25C; (b)Two charge/discharge cycles under bending and flat condition at 0.25C (c,d) hand held bending test for working voltage comparison.

The battery's electrochemical performance under repeating bending was further tested. As showed in Figure 3.6, the galvanostatic charge/discharge profile only shifts to leave a little after 1000 times bending. The capacity retention is more than 86% after 1000 times bending. This result demonstrate that the battery can tolerate the bending and remain good electrochemical performance.

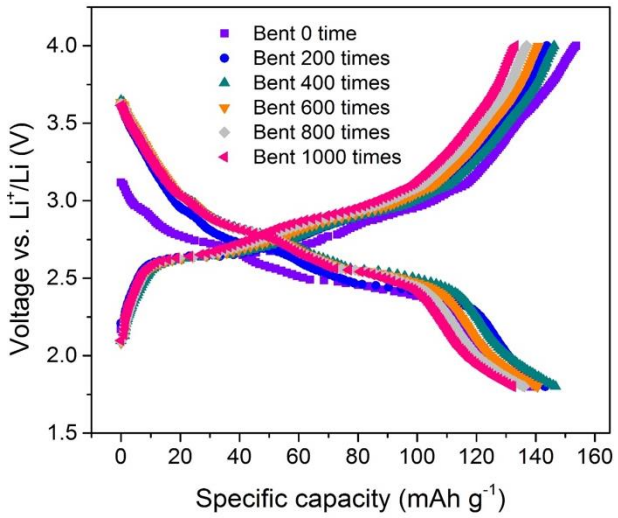

Figure 3.6 Galvanostatic charge/discharge test under repeating bending. The battery was tested at 1C.

The cycling stability of the battery was further tested. As shown in Figure 3.7, the initial capacity can be 150 mA h g-1 at 1C. After 20cycles, a slow degrade was presented. Around 90 mA h g-1 can be remained after 400 cycles, indicating a relatively good stability during the cycling. The coulombic efficiency was only around 90% at the first cycle, which is quite common in lithium-storage electrodes due to formation of some solid-electrolyte interface (SEI). Other than that, the coulombic efficiency reached ~100% from the second cycle and remains until the end, suggesting a high reversibility.

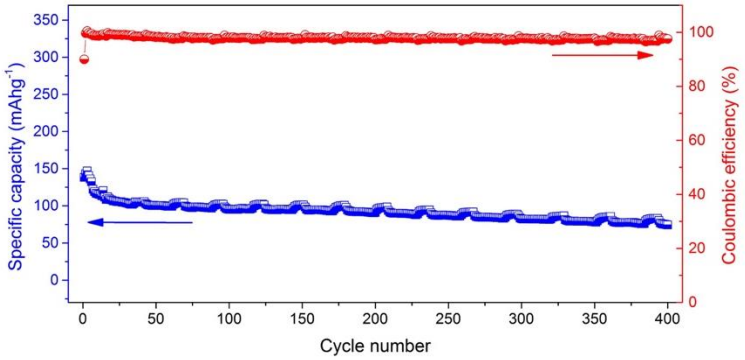

Figure 3.7 Cycling performance test of the CNT/V2O5 composite with 25wt % CNTs under 1C condition.

3.3 conclusion

In summary, we reported a facile and cost-effective fabricating strategy for the V_2O_5/CNT composite interpenetration network as high mechanical strength electrode material for flexible lithium-ion batteries. In our work, *in-situ* fibrillated PTFE can be incorporate into the existing network with simple kneading method and provide a sturdy support for the robust framework via its self-interconnection. Although the practical capacity of the composite matrix might still need improvement, the superior mechanical strength has already surpassed most of its competitors. With a young's modulus at 800 MPa, this cathode sheet can sustain tremendous amount of bending without impact on performance.

3.4 Experiment Section

Synthesis of CNTs/V_2O_5 nanocomposites

At the preliminary stage of the study, multi-wall carbon nanotubes (CNTs) were firstly functionalized to attach carboxylic groups on its surface using method similar to Gao. Then followed by similar hydrothermal method of Xiong, the composite was synthesized. Briefly,

certain amount of CNTs were acid treated and then mix with 0.15g ammonium metavanadate (NH_4VO_3), 0.5ml 2M HCl solution and 0.25g of surfactant P-123 ($EO_{20}PO_{70}EO_{20}$), where EO and PO are ethylene oxide and propylene oxide, respectively. After ultrasonication for 30mins, stir the mixture for 12 hours, then transferred into 100ml Telflon-lined autoclave and heated to 120 ^oC for 24 h. The final precipitates were rinsed with water, acetone under filtration and then vacuum dried. The amount of CNTs used were varied from 0.037, 0.061 to 0.09g, resulting in composites with 20, 33 and 50 wt-% of the CNTs, respectively.

Preparation of CNTs/V_2O_5 nanocomposite sheet

After synthesis V_2O_5/CNT nanocomposites with hydrothermal approach, the product was washed and then vacuum dried overnight. The final product was then put into the grinder accompanied with 10-wt% PTFE solution for grinding while using ethanol as dispersion agent. After obtained a solid flexible electrode material from grinding about 30mins, place the material on flat surface and apply shear force by repeat rolling and folding process until the material became a flat sheet. At last, 300^oC of hot press was performed to obtain an approximate 120um thickness sheet.

Characterization

The X-ray diffraction patterns were obtained from a Rigaku Miniflex II diffractometer using Cu Kα radiation operated at 30kV and 15mA. SEM morphology of the samples were obtained by a field-emission scanning electron microscopy (FEI Nova 230).

Electrochemical Measurements

The electrochemical performance was evaluated using CR2032 coin-type cells. Coin-type

half-cells were assembled in an argon-filled glove box with the composites mentioned in this paper as the positive electrode and Li metal foil as the counter and reference electrode. A Celgard 2400 membrance was used as the separator and 1 M $LiPF_6$ solution in ethylene carbonate (EC) and diethyl carbonate (DEC) mixed at weight ratio of 1:1 was used as electrolyte with 5% of fluoroethylene carbonate (FEC). Galvanostatic cycling tests were tested using a Land battery test system (Wuhan Land Electronic Co., China) with cut-off voltages of 1.8–4.0 V versus Li/Li^+ at room temperature.

Mechanical Measurements

Tensile tests were conducted on INSTRON 5564 at 1.0 mm/min with a strain rate of 1% min^{-1} and a 1 cm gauge length.

Chapter 4 Gel electrolyte for flexible battery

With the rapid increasing demand of the flexible batteries, various types of electrolyte system have been developed in order to fulfill the requirement of both high safety and high mechanical strength. Compare with liquid electrolytes that consist of high content of flammable solvents and solid-state electrolytes that suffered from low ionic transportation, gel polymer electrolytes have become the most promising candidate for flexible lithium batteries. However, low ionic conductivity and sluggish Li^+ transport of polymer electrolytes is still a restriction towards their applications. Here metal-organic framework (MOF) containing open-metal sites (OMSs) are used as fillers that endow GPL with simultaneously high ionic conductivity (> 1 mS cm^{-1}) and Li^+ transference number (up to 0.66), which results from immobilized anions and facilitated cation conduction by virtue of OMSs. Implementations of the GPL with OMSs-laden MOF in pseudo-

solid-state batteries significantly facilitates the ion transportation in Li-ion batteries (LIBs), which further the implication of GPL in flexible batteries.

4.1 Introduction

The rapid-growing market of portable electric applications has stimulated intensive research on flexible LIBs with high energy density, long cycling life and good safety. Conventional LIBs, primarily based on intercalation electrodes coupled with organic liquid electrolytes, suffer from the limited theoretical energy density and safety risks of leakage and flammability, struggling to completely fulfill the demand.[72, 73] Solid-state electrolytes could largely solve these challenges by circumventing the electrolyte leakage and adopting high-energy metallic Li anode.[44, 74] The glass-/ceramic-based electrolytes as prevailing categories of solid-state electrolytes possess significant advantages in ionic conductivity (10^{-2} S cm^{-1}) and mechanical strength. However, their scaled processability and interfacial resistance with electrodes are the formidable obstacles to practical implementation.

As an alternate category, solid polymer electrolytes comprising polymers (e.g., polyethylene oxide, PEO) and lithium salts feature decent processing flexibility while poor ionic conductivity ($10^{-8} - 10^{-5}$ S cm^{-1}), rendering their prospects less intriguing.[75-77] To ameliorate such issue, gel polymer electrolytes imbibed with organic solvents (plasticizers) and/or incorporated with

inorganic solid fillers (e.g., SiO_2, TiO_2) have been effectively demonstrated to boost ion conductions, where the plasticizers and filler serve to dissociate lithium salts and reduce the crystallinity of the polymer.[78, 79] Nevertheless, the non-conductive solid fillers block the ion-translocation pathways that potentially limit interfacial engineering and compatibility with electrodes.[80, 81]

Particular attention was given to metal-organic frameworks (MOFs) as an emerging class of microporous filler. The MOFs periodically built from metal clusters and organic ligands, provide an excellent platform of functional materials for tuning ion-transport behaviors. Analogous to the solid fillers, prior studies have reported the use of MOFs (Al/Zn/Ni/Mg-based) as fillers for PEO-based solid polymers.[82-85] However, few studies have revealed that the MOFs could alter Li^+ ion transference number (t_{Li^+}), which is referred to as the fraction of Li^+ ion conductivity to overall ionic conductivity. The reported low t_{Li^+} of the electrolytes with MOF fillers (< 0.4) signifies that only a small portion of ion-conduction carries the effective Li^+ ion conduction. The transport limitation during battery operation induces local depletion of Li^+ ions that aggravates concentration polarization, deteriorates interfacial stability, and cycle lifespan.[86] More recently, post-synthetic modifications endow a Zr-based MOF with charged ligands for immobilizing anions, and the resulting MOF-laden polymer electrolytes afford superior t_{Li^+} above 0.7.[87] However, poor efficiency of this artificial modification leads to moderate conductivity ($10^{-4} - 10^{-5}$ S cm^{-1}) and high activation energy (> 0.3 eV), which are detrimental to high-rate and low-temperature operations of LIBs.

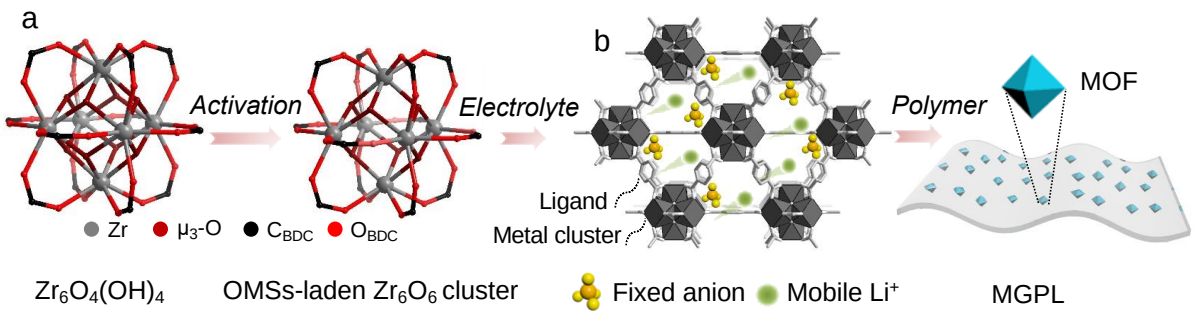

Figure 4.1 Illustrative drawings: (a) thermal activation of a Zr-based MOF (UiO-66) generates OMSs that tether anions while facilitating Li^+-ion conduction in gel polymer electrolyte.

Herein, we rationally design and employ a Zr-based MOF possessing OMSs as the microporous fillers for GPLs (Figure 4.1a). Compared with those reported polymer electrolytes comprising MOFs, the present UiO-66 provides thermally generated OMSs with Lewis acidity that can readily anchor anions and facilitate cation (Li^+) conduction (Figure 4.1b), which simultaneously afford high ionic conductivity in 1.52×10^{-3} S cm^{-1}, high t_{Li^+} up to 0.66 and low activation energy below 0.1 eV. Such facile treatment of a Zr-based MOF endows gel polymer electrolyte with desirable ion-transport attributes that guarantee the safe and durable operation of batteries, thereby demonstrating a new class of filler additive for high-performance polymer electrolytes.

4.2 results and discussions

Structural Properties

The Zr-based MOF, namely UiO-66, is made by coordinating $Zr_6O_4(OH)_4$ octahedron clusters with 1,4-benzenedicarboxylic acid (BDC) ligands, generating highly microporous scaffolds with structural rigidity and thermal stability. In this work, UiO-66 (Zr) was firstly synthesized by one-step hydrothermal reaction. Figure 4.2 (a-b) shows a scanning electron spectroscopy (SEM) image of UiO-66 synthesized according to well-reported literature,[88] where the MOF exhibits octahedral-shaped morphology and uniform particulate size of 200 nm.

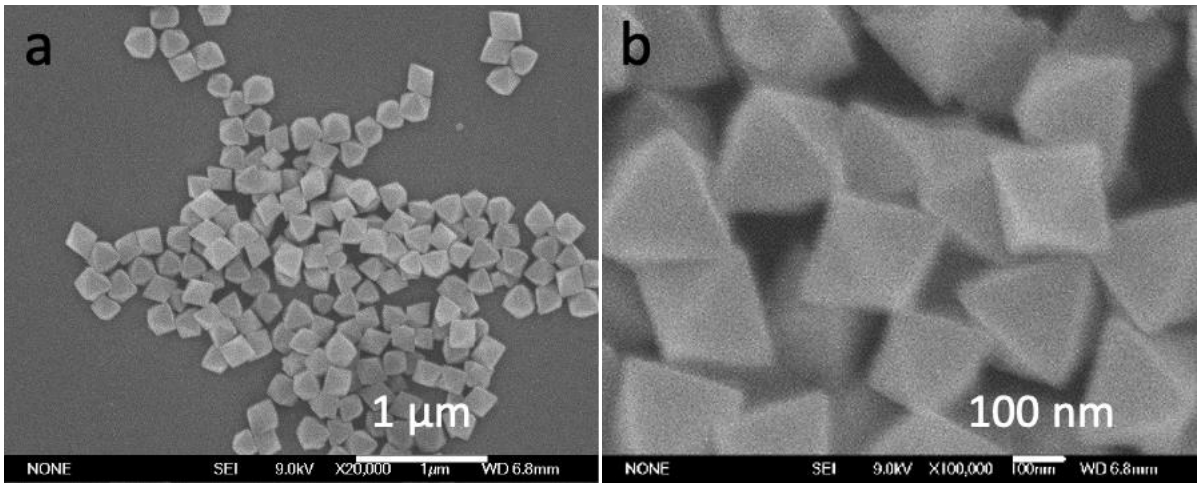

Figure 4.2(a-b) SEM image of UiO-66 synthesized

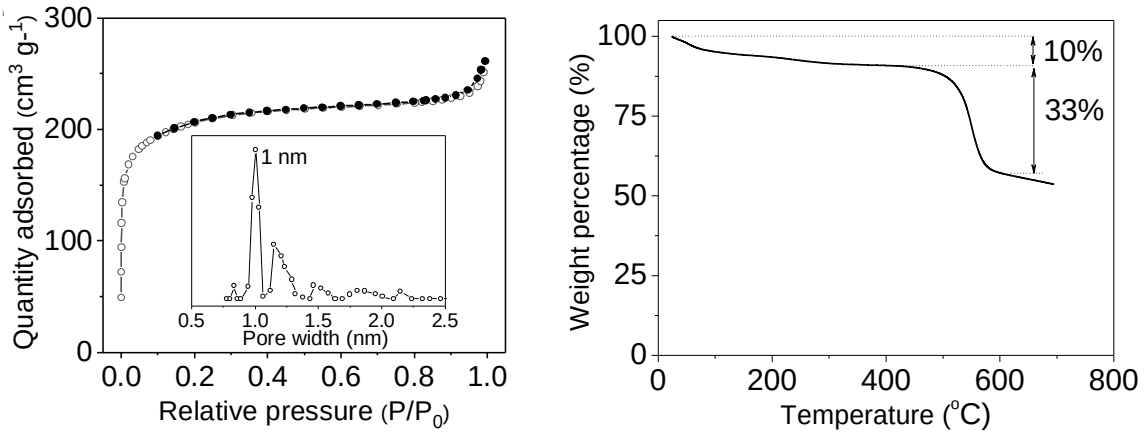

Figure 4.3 (a) TGA curve of UiO-66 in N_2 atmosphere. (b) N2 isotherms of UiO-66 and pore size distribution (inset).

As shown in Figure 4.3a, N_2 adsorption/desorption isotherms and corresponding pore size distribution (Density-Function Theory) curve indicate a huge BET (Brunauer-Emmett-Teller) surface area of 683 m^2 g^{-1} and a dominant micro-pore size at 1 nm, respectively.

The thermogravimetric analysis (TGA) verifies the superior thermal stability of UiO-66.[89] As shown in Figure 4.3b, the sample exhibits a progressive weight loss reaching a plateau at ~ 300 °C, which could be attributed to the removal of guest molecules and departure of capped hydroxyl groups (Zr–OH) on Zr^{4+} (from $Zr_6O_4(OH)_4$ to Zr_6O_6-based metal nodes). A subsequent sharp loss of 33% after 400 °C is associated with the decomposition of the ligands. The activation process was thus performed at 300 °C to expose OMSs via dihydroxylation.[90]

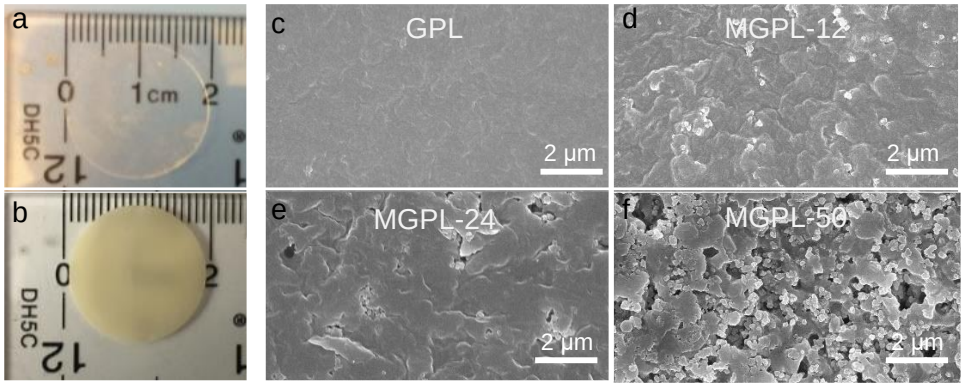

Figure 4.4 Photographs are showing freestanding and leakage-free (a) GPL and (b) MGPL membranes. (c-f) SEM images of GPL and MGPLs.

A conventional gel polymer electrolyte denoted as GPL employs poly (vinylidene fluoride-co-hexafluoropropylene) (PVDF-HFP) as the polymeric matrix and $LiClO_4$ in propylene carbonate (PC) as the electrolyte. Figure 4.4a presents a photograph of GPL that could be prepared as a freestanding membrane with leakage-free and transparent appearances, which turn into pale-yellow after incorporating the MOF. The MOF-mediated GPL comprises activated MOF particles in uniform combination with GPL, where the OMSs-abundant MOF nanoparticles function as the ion-transport regulators immobilizing diffusive anions and facilitating conduction of lithium-ions. The composite gel polymer electrolyte is hereinafter designated as MGPL-X, where the X represents the content ratio of MOF particles (e.g., MGPL-12 stands for 12 wt-% particle loading).

The microstructures of electrolyte membranes were imaged by SEM (Figure 4.4c-f). As shown in Figure 4.4c, the GPL membrane exhibits a homogenous and smooth surface with dense bulk texture. In comparison, the micrographs of MGPL-12 (Figure 4.4d), MGPL-24 (Figure 4.4e), and MGPL-50 (Figure 4.4f) reveal increasing surface roughness and porosity along with the increasing MOF loading. In particular, MGPL-50 with the highest loading shows discernable particulate morphology.

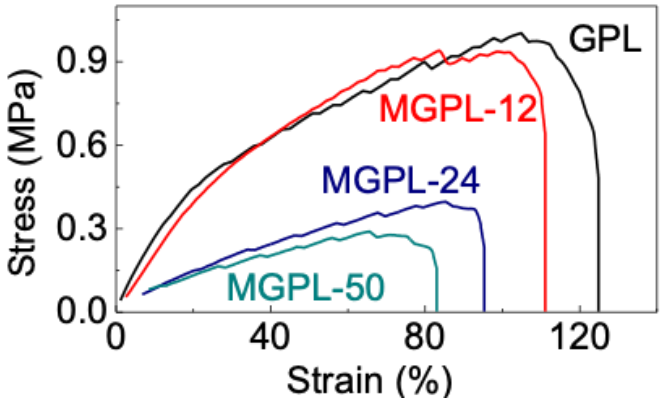

Figure 4.5 Young's module mechanical test with different w% of MOFs additive.

Table 4-1 Mechanical performance of GPL and MGPLs.

Sample	Stress (MPa)	Strain (%)	Modulus (MPa)
GPL	1.23 ± 0.35	138.7 ± 21.2	2.03 ± 0.6
MGPL-12	1.09 ± 0.46	101.3 ± 28.7	2.03 ± 0.25
MGPL-24	0.39 ± 0.04	92.4 ± 2.8	0.66 ± 0.09
MGPL-50	0.27 ± 0.03	76.3 ± 8.3	0.46 ± 0.04

The mechanical property of electrolyte membranes (~ 80 μm) was assessed by the stress-strain test. As shown in Figure 4.5 and summarized in Table 1.1, the GPL manifests the highest tensile strength of 1.23 MPa with elongation of 138.7% and Young's modulus of 2.03 MPa. The MGPL observes a downward trend over tensile strength with the increasing MOF loading. In particular, MGPL-12 provides a tensile strength of 1.09 MPa and Young's modulus of 2.0 MPa, which are comparable to the mechanical strengths of GPL.

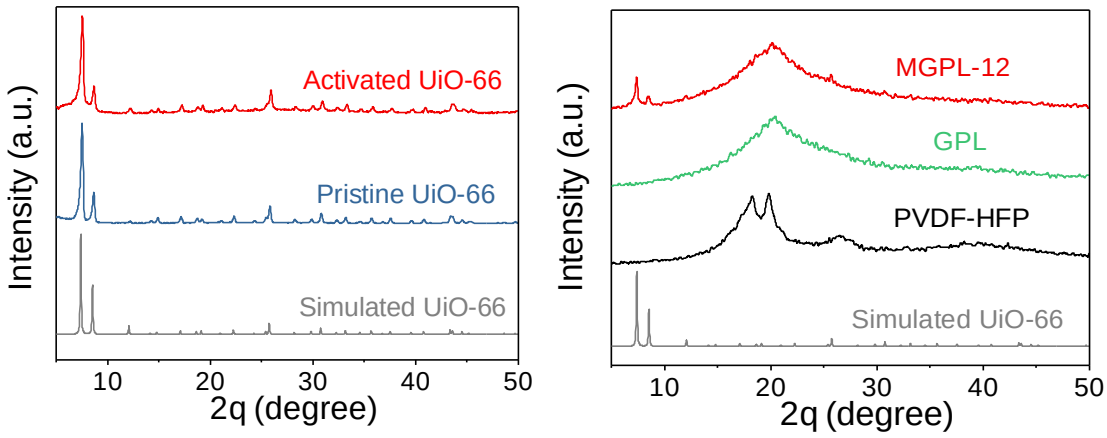

Figure 4.6 (a) XRD patterns of simulated, pristine, and activated UiO-66. (b) XRD patterns of simulated UiO-66, PVDF-HFP powders, GPL, and MGPL-12.

The structural evolutions of electrolyte membranes were further probed by X-ray diffraction (XRD) and infrared spectroscopy (IR). Figure 4.6(a-b) compares XRD patterns of MOF, polymer, GPL, and MGPL. The pattern of the MOF manifests preserved crystalline structure after thermal activation (Figure 4.6a). As shown in Figure 4.6b, three prominent diffraction peaks of PVDF-HFP powders at 18.2°, 19.8°, and 26.5° indicate the existence of α-phase, which turns into β-phase signified by an exclusive broad peak at 20.3° upon gelation with liquid electrolyte (GPL). The semi-crystallinity of PVDF-HFP in GPL affords both mechanical strength and high ambient ionic conductivity, which originate from the rigid support by crystal VDF and trapped electrolyte by amorphous HFP, respectively.[91] Accordingly, the pattern of MGPL-12 encompasses both characteristic peaks of the MOF and the β-phase of PVDF-HFP.

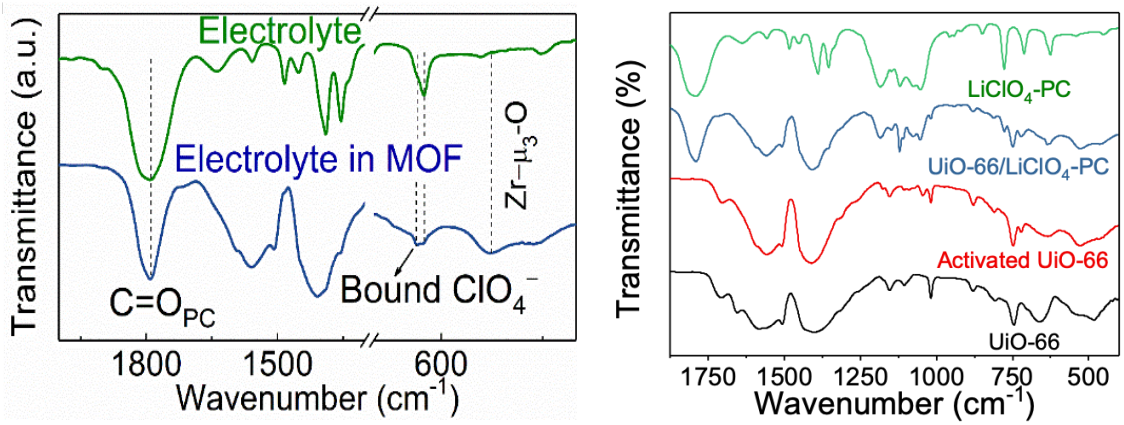

Figure 4.7 (a)IR spectra of UiO-66, activated UiO-66, liquid electrolyte (1 M $LiClO_4$ in PC) and (b)electrolyte-infiltrated UiO-66.

Figure S4 displays the IR spectra of the pristine and activated MOF, where the dihydroxylation and emergence of Lewis acidic OMSs are evidenced by the disappearance of the band at 479 cm^{-1} for (HO)–Zr–(OH) bending mode.[92] Meanwhile, the structural integrity of the activated MOF is supported by signals locating at 1410 cm^{-1} and 530 cm^{-1} for ligand (BDC) and metal clusters (Zr–O), respectively. Impregnating liquid electrolyte ($LiClO_4$ in PC) into MOF particles reveals that the confined electrolyte species exhibit distinct vibrations compared to the parent liquid phase. As shown in Figure 2h, anion (ClO_4^-) enclosed in MOF exhibits an additional vibration at 635 cm^{-1} besides its symmetric component at 626 cm^{-1}, indicating the partial asymmetric configuration of bound anions in the activated MOF.[93] As for PC solvent, a board peak at 1793 cm^{-1} ascribed to carbonyl (C=O) turns into a sharp one peaking at 1790 cm^{-1}, hinting stronger solvation by PC trapped in MOF. The above bonding information collectively suggests an ion-regulating effect by particulate MOF fillers in the GPL.

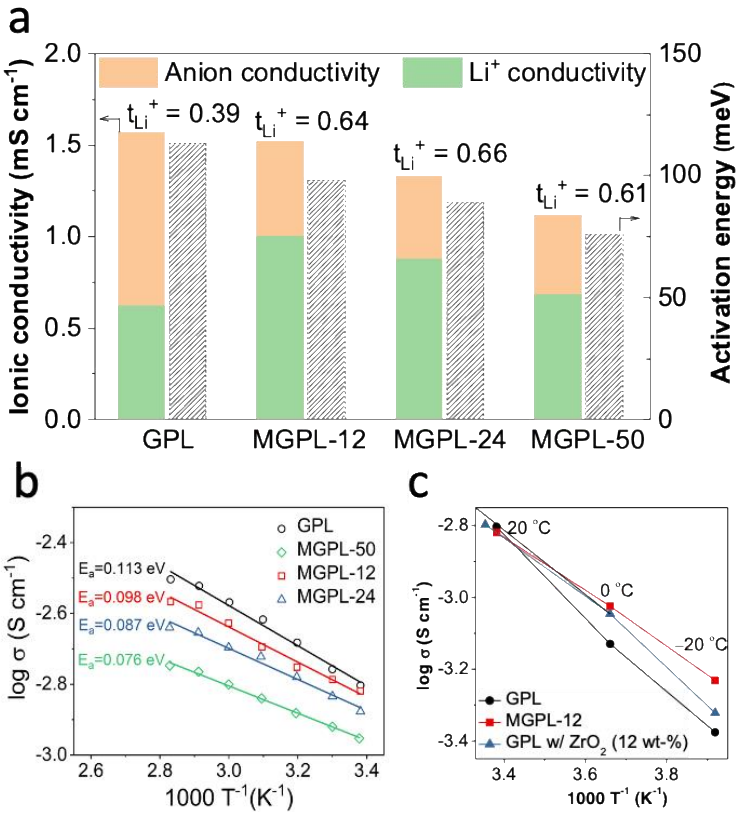

Figure 4.8 (a) Ambient ionic conductivity and thermal activation energy of electrolyte membranes, where the cation and anion conductivities partitioned on the basis of t_{Li}^{+}. (b) Comparisons of activation energy between MGPL-X and GPL control group. (c) Low-temperature (0, –20 °C) conductivity of GPL, MGPL-12, and GPL with 12% wt-% ZrO_2.

The ionic conductivity of electrolyte membranes was measured by electrochemical impedance spectroscopy (EIS) using identical stainless-steel disks as blocking electrodes. Meanwhile, ionic conductivities equilibrated at temperatures ranging from 20 to 80 °C were also collected and linearly fitted by the Arrhenius equation for thermal activation energy. As shown in Figure 4.8(a-b), the ambient ionic conductivity of GPL, MGPL-12, MGPL-24, and MGPL-50 exhibits a downward trend of 1.57, 1.52, 1.33, and 1.11 mS cm^{-1}, respectively. Such a phenomenon could be interpreted by the elevated transport tortuosity introduced by framework skeletons. However, the activation energy shows a decreasing trend of 113, 98, 87, and 76 meV with increasing content of

MOF particles, implying that the OMSs-containing MOF particles ease the diffusion energy barrier. Such facilitated ion-conduction was further supported by ionic conductivity at the low-temperature. As shown in Figure 4.8c, the MGPL-12 exhibits superior ionic conductivity of 0.59 mS cm^{-1} at –20 °C, notably exceeding 0.42 mS cm^{-1} from GPL and 0.48 mS cm^{-1} from GPL with conventional ceramic fillers (12 wt-% ZrO_2). It is noted that the MGPL-12 affords analogous ionic conductivity and mechanical strength, as well as lower activation energy than GPL, affording a suitable MGPL for electrochemical performance evaluations.

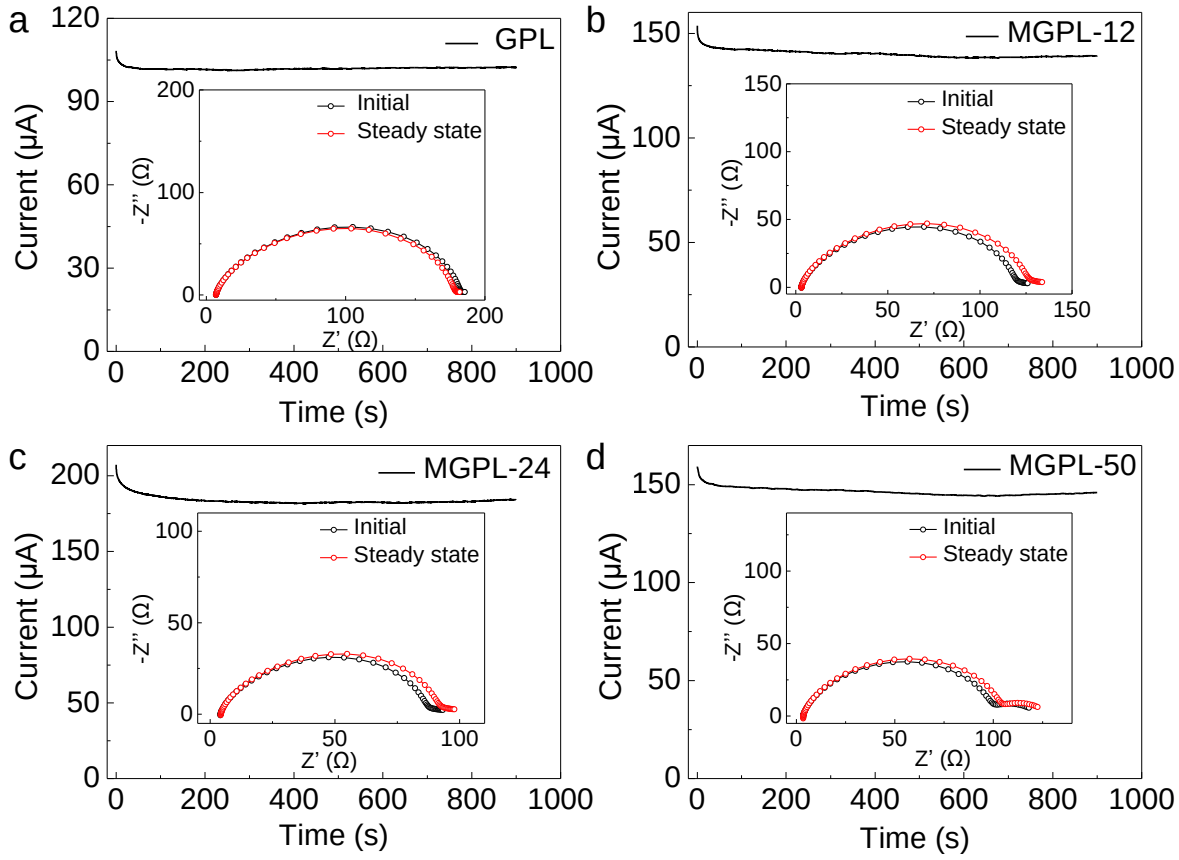

Figure 4.9 Measurements of t_{Li^+} on the basis of a potentiostat approach.

As another pivotal electrolyte property, t_{Li^+} serves to evaluate Li^+ transport efficiency and predict the degree of ion-concentration polarization during battery operation. Symmetric Li (Li|Li) cells sandwiching electrolyte membranes were fabricated for measuring t_{Li^+} by a well-established

potentiostatic polarization method (Figure 4.9). [94] The derived t_{Li^+} of 0.39 for GPL is in good accordance with reported literature.[95] With incorporation of MOF particles, the t_{Li^+} of MGPL-12, MGPL-24 and MGPL-50 is appreciably improved to 0.64, 0.66, and 0.61, respectively. As summarized in Figure 4.8a, all MGPLs yield enhanced Li^+ conductivity (product of t_{Li^+} and ionic conductivity) despite the slightly decreased overall ionic conductivity compared with GPL.

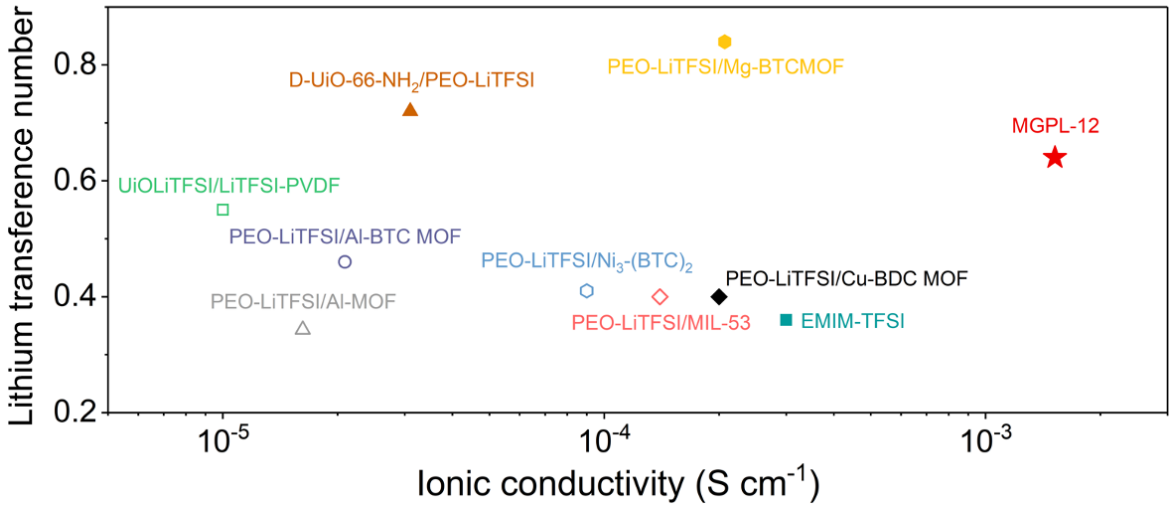

Figure 4.10 Ionic conductivty comparison between MGPL-12 and reported GPLs.

Of particular, the high ionic conductivity and t_{Li^+} of MGPL-12 are among the best recently reported polymer electrolytes involving MOFs (Figure 4.10) [82, 83, 85, 87, 96-103] and other fillers (Table 4-2). The surpassing transport efficiency could be attributed to the OMSs-lined microporous channels, which impose confinement and complexation to the free anions as well as promote the preferential transport of Li^+ ions. [101, 104, 105]

Table 4-2. Conductivity and Li^+ transference number comparisons between polymer electrolytes with various filler materials

Electrolyte system	Conductivity (S cm^{-1})	Temperature (^oC)	t_{Li^+}	Ref.
MGPL-12	1.52×10^{-3}	25	0.64	This work
[EMIM][TFSI]-LiTFSI-(MOF-525)	3×10^{-4}	25	0.36	[106]
PEO-LiTFSI-PC-SiO_2	5×10^{-3}	25	n/a	[107]
PEO-LiTFSI-LLTO	5.53×10^{-5}	25	0.195	[108]
PAN-$LiClO_4$-LLTO	2.4×10^{-4}	25	n/a	[109]
LiTFSI-[Py_{13}][TFSI]-SiO_2	1.37×10^{-3}	30	0.22	[110]
PEO-LiTFSI-LLZO	2.5×10^{-4}	25	n/a	[111]
PEO-LiTFSI-LLZTO	1.12×10^{-5}	25	0.58	[112]
$LiClO_4$-PVDF-LLZTO	5×10^{-4}	25	n/a	[113]
PEO-LiTFSI-Cationic (UiO-66-NH_2) (12.5 vol%)	3.1×10^{-5}	25	0.72	[87]
PEO-LiTFSI-(Mg-BTC) (10 wt%)	2×10^{-4}	30	0.4	[85]
PEO-LiTFSI-(MOF-5) (10 wt%)	3.16×10^{-5}	25	n/a	[114]
PVDF- LiTFSI-(UiO-LiTFSI) (56 wt%)	2.07×10^{-4}	25	0.84	[98]
PEO-LiTFSI-(Al-BTC) (10 wt%)	$\sim 1 \times 10^{-5}$	30	0.55	[103]
PEO-(BMIM-PF_6)-(Cu-BTC)	5.3×10^{-4}	25	n/a	[115]
PEO-LiTFSI-(Al-MOF) (5 wt%)	2.09×10^{-5}	30	0.46	[116]
PEO-LiTFSI-(MIL-53) (10 wt%)	1.62×10^{-5}	30	0.34	[117]
PEO-LiTFSI-(Ni-BTC) (10 wt%)	1.4×10^{-4}	30	0.4	[118]
PEO-LiTFSI-(Cu-BDC) (10 wt%)	9×10^{-5}	30	0.41	[119]

PVDF-(MOF-74)	6.72×10^{-4}	25	0.66	[100]
PEO-$LiPF_6$-(UiO-66)	1.47×10^{-4}	30	0.47	[97]
[EMIM][TFSI]-PEO-(UiO-66)	1.3×10^{-4}	30	0.35	[99]

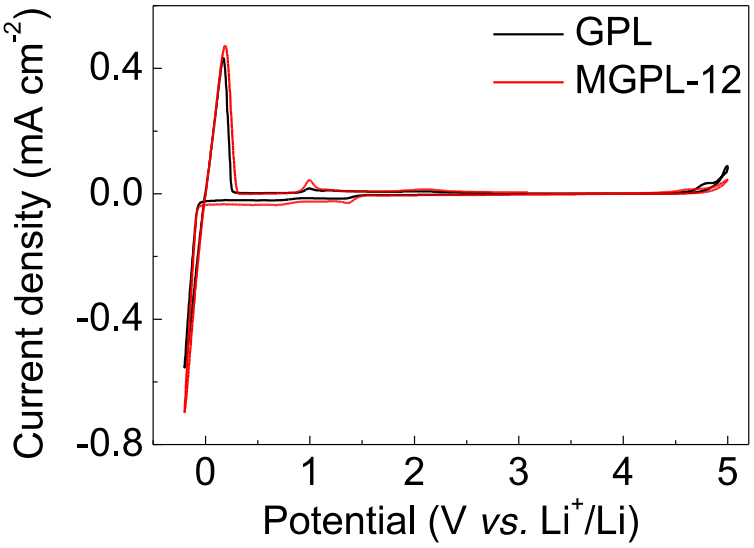

Figure 4-11 CV curves of GPL and MGPL-12 sandwiched by Li metal and stainless-steel electrodes.

The electrochemical stability window of electrolyte membranes was evaluated by cyclic voltammetry (CV) using stainless-steel as a working electrode and Li metal as a counter/reference electrode. As plotted in Figure 4-11, the CV curves of cells using GPL and MGPL-12 show

reversible Li/Li^+ stripping-plating processes on steel electrodes (between –0.2 V and 0.2 V, vs. Li/Li^+), and irreversible moderate oxidation peaks beyond 4.4 V, which demonstrate the electrochemical stability of MOF particles and a feasible working window for practical batteries.

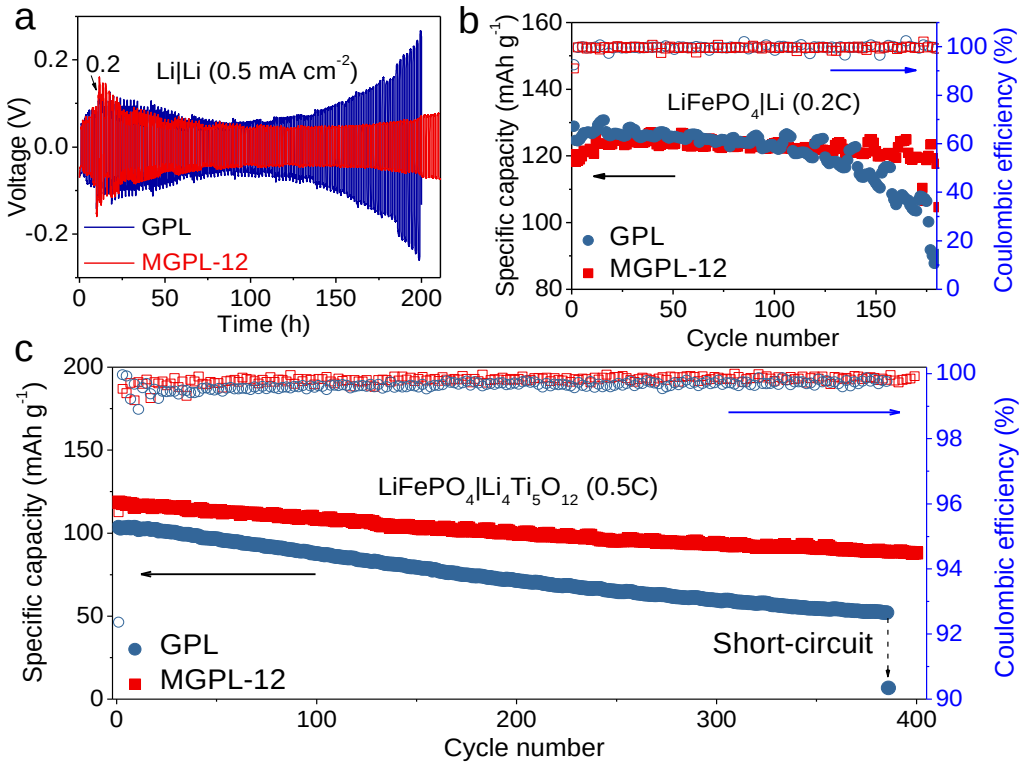

Figure 4.12 (a) Polarization tests of Li|Li cells (200 h) under 0.5 mA cm^{-2} with a time interval of 1 h (0.2 mA cm^{-2} was applied for the first 10 h). (b) Galvanostatic cycling of pseudo-solid-state Li-metal cells ($LiFePO_4$|Li) under 0.2C. (c) Galvanostatic cycling of pseudo-solid-state Li-ion cells ($LiFePO_4$|$Li_4Ti_5O_{12}$) under 0.5C

The long-term electrochemical stability of electrolyte membranes (GPL and MGPL-12) against Li metal was investigated by the galvanostatic cycling of Li|Li cells (Figure 4.12a). At the initial stage, both cells show similar overpotentials at 0.2 mA cm^{-2} with a time interval of 1 h (for total 10 h). After 10 hours' operation, the cells were polarized at a higher current density of 0.5 mA cm^{-2}, yielding stabilizing overpotentials of 40 mV and ~ 60 mV after 110 h for the cell with MGPL-12 and GPL, respectively. Afterward, the cell using GPL suffers from gradually escalating overpotential as indicated by a cell voltage built-up from 50 mV at 110 h to 280 mV at 200 h. In

marked contrast, the cell using MGPL-12 maintains a considerably smaller overpotential of 72 mV after 210 h without a cell failure.

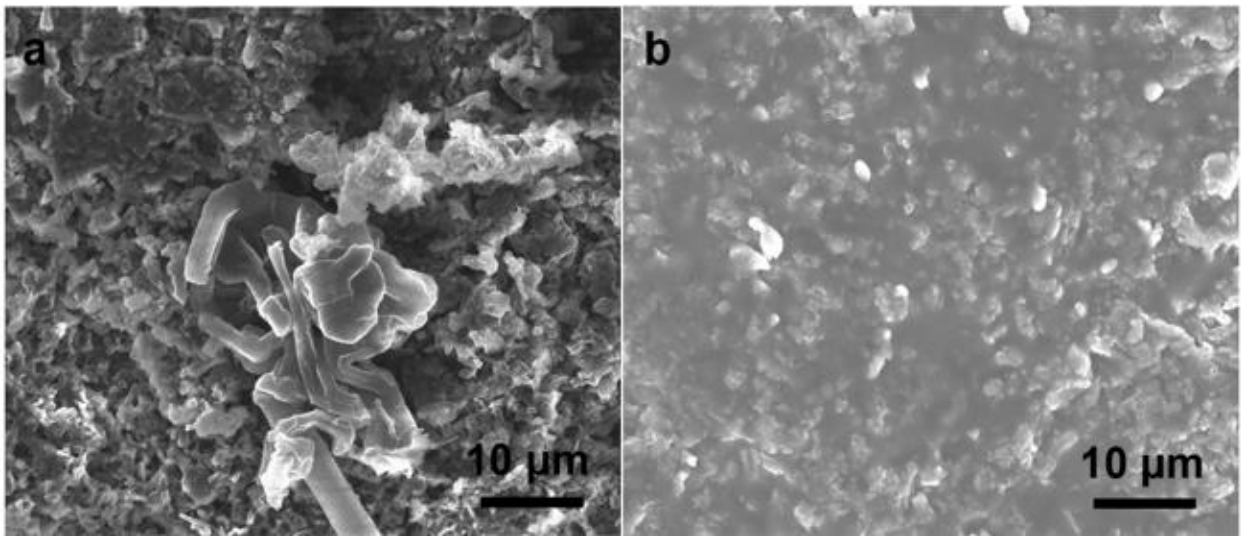

Figure 4.13 SEM images of Li metal surface after cycling test (100 cycles) at 0.5 mA cm^{-2} with a deposition capacity of 0.5 mAh cm^{-2}. (a) Li metal surface of the cell with GPL. (b) Li metal surface of the cell with MGPL-12.

The post-cycle morphology of Li electrodes was examined by SEM imaging, which confirms a filamentous surface from the Li electrode harvested from the cell using conventional GPL (Figure 4.13). Consistently, the cycled Li electrode coupled with MGPL-12 shows less porous surface without protruded morphology, indicating that the MOF particles suppress the interfacial degradation between GPL and metallic Li.

The application assessment of electrolyte membranes (GPL and MGPL-12) for pseudo-solid-state batteries was conducted using $LiFePO_4$ as the cathode material, and Li or $Li_4Ti_5O_{12}$ as anode materials. Figure 4b shows galvanostatic cycling of prototype pseudo-solid-state Li-metal cells comprising $LiFePO_4$ and Li ($LiFePO_4$|Li, 0.2C, 2.5-4 V), where the cells using GPL and MGPL-

12 deliver almost identical and stabilized specific capacity of 122 mAh g^{-1} for the first 100 cycles. Afterward, the cell using GPL initiates an accelerating capacity fade with 87 mAh g^{-1} retained by the end of 180 cycles. While the cell using MGPL-12 robustly affords 120 mAh g^{-1} at the same end condition. The cycling results involving Li are in good agreement with the polarization tests of symmetric Li cells, again proving that the facilitated Li^+-ion conduction by MOF fillers benefits constructing affinitive interfaces between GPL and Li. Furthermore, pseudo-solid-state Li-ion cells (1-3 V) combine $LiFePO_4$ cathode, and $Li_4Ti_5O_{12}$ anode was fabricated for validating cell durability adapting MGPL. The cell cycle stability at 0.5C was compared in Figure 4c. The cell using MGPL-12 delivers a discharge capacity of 88 mAh g^{-1} after 400 cycles, which corresponds to an exceptional capacity retention of 75% and an average Coulombic efficiency of 99.9%. In sharp contrast, the cell using GPL affords a lower average efficiency of 99.6% during the test period. Furthermore, only 50% of its original capacity was retained after 385 cycles (52 mAh g^{-1}), and the cell was terminated due to a short-circuit failure, which stems from the poor transport efficiency of GPL that leads to concentration polarization and fails to inhibit penetration of dendritic Li.

4.3 conclusion

In summary, we have employed functional UiO-66 nanoparticles as the filler and PVDF-HFP as the host to construct a new hybrid membrane, where the tune of ionic transport is realized by the interaction between anions and unsaturated Zr^{4+} sites of UiO-66, meanwhile, the constant ion concentration is achieved due to the homogeneous physical structure and uniform particle distribution. This specific chemical regulation of ions enables high Li^+ transport efficiency and good interface electrochemical stability, thus leading to promising electrochemical performance in solid-state lithium batteries. As a result, both LMBs and LIBs exhibit outstanding battery performance. In addition, we conclude that such chemical adsorbent is an effective strategy to improve electrolyte properties and increase lifetime of Li metal anode. The exclusive insight into structural optimization of electrolytes with high Li^+ transport efficiency and good interfacial compatibility will provide new avenues for further rational design of solid-state electrolyte systems.

3.4 experimental section

Prepare UiO-66. Terephthalic acid (10 mmol, 1.66 g) was dissolved in DMF 180 mL, benzoic acid (10 equiv with respect to $ZrCl_4$) and concentrated HCl (1.65 mL) were added into the solution. The solution was stirred at room temperature for 0.5 h, then $ZrCl_4$ (10 mmol, 2.33 g) was dissolved in the solution. The reaction vessel was transferred to an oven and heated at 120 ^oC for 72 h. The

solution was cooled to room temperature and the precipitates were isolated by centrifugation. The solids were suspended in DMF and stirred overnight. The suspension was centrifuged and solid was washed with DMF for five times. The obtained solid was washed with methanol in the same way as described for washing with DMF. Finally, the solid was dried at 60 ^{o}C overnight under vacuum.

Prepare hybrid polymer gel electrolyte. Take one composition with UiO-66 accounts for 12% as an example. UiO-66 was first activated at 300 ^{o}C for 24 h and then transferred to glove box. UiO-66 (63 mg) was immersed in 1 M $LiClO_4$-PC (1.2 mL) electrolyte overnight, then 6 mL dimethyl carbonate (DMC) was added. The suspension was stirred for 6 h, then poly(vinylidene fluoride-co-hexafluoro propene) (PVDF-HFP) (460 mg) was added into the suspension. The mixture was stirred at 60 ^{o}C overnight. 1.5 mL suspension was taken and casted on a polypropylene (PP) plate. After the evaporation of the solvent, the composite polymer gel electrolyte can be obtained. Pure polymer gel electrolyte was prepared as the same method only without the addition of UiO-66.

Characterization. XRD was tested by a Rigaku powder X-ray diffractometer. Fourier Transform Infrared Spectroscopy (FTIR) data were recorded on a Nicolet 6700 FTIR. SEM images were taken using FEI Nova 230. X-ray photoelectron spectroscopy (XPS) characterization was tested by using a Kratos AXIS ULTRADLD XPS system equipped with an Al Kα monochromated X-ray source. For XPS tests of SEI layer, the batteries were tested 100 cycles at 0.5 mA cm^{-2} with deposition of 0.5 mA h cm^{-2} and disassembled in glove box. The Li metals were sealed in a transporter in the glove box before being quickly transferred to the high-vacuum chamber of XPS (AXIS Ultra DLD) for analysis. The binding energy values were all calibrated using C 1s peak at 284.8 eV. Thermogravimetric analysis (TGA) was tested using TA instruments Q500. Mechanical

tensile-stress experiments were carried out using an Instron 5942 at a strain rate of 5 mm min^{-1}.

Electrochemical measurements. Ionic conductivity test was measured in a coin cell with structure stainless steel (SS)| gel electrolyte |SS structure. Alternating current (AC) impedance spectroscopy was used and the frequency range was 500 kHz to 1 Hz with a voltage amplitude of 10 mV in the temperature range from room temperature to 80 ^{o}C. The conductivity σ was calculated according to the equation:

$$\sigma = \frac{L}{RA}$$

L (cm) is thickness of gel, R (Ω) is resistance tested by AC impedance spectroscopy and A (cm^2) is the area of stainless steel.

Potentiostatic polarization method was used to test the transference number. Li metal | electrolyte | Li metal cells were utilized to test t_+ and t_+ was calculated by the following equation:

$$t_+ = \frac{I_s(\Delta V - I_0 R_0)}{I_0(\Delta V - I_s R_s)}$$

ΔV is the voltage polarization, applied voltage is 20 mV, I_0 and R_0 are the initial current and resistance, I_s and R_s are the steady state current and resistance, respectively.

The batteries were tested using 2032 type coin cells. No matter in Li symmetric cells or $LiNi_{1/3}Co_{1/3}Mn_{1/3}O_2$-Li metal cells, composite polymer gel electrolyte was directly used without further addition of liquid electrolyte. Galvanostatic charge–discharge experiments were carried out with a LAND battery testing system. The cyclic voltammetry was performed on VMP3 Potentiostat/Galvanostat (Princeton Applied Research). The electrochemical impedance spectroscopy (EIS) was tested with Solartron.

Cathode material ($LiNi_{1/3}Co_{1/3}Mn_{1/3}O_2$ or $LiFePO_4$) was mixed with conductive carbon and polyvinylidene difluoride (PVDF) in a mass ratio of 80:10:10. Then N-methyl-2-pyrrolidone (NMP) was added into the solid powder to get the slurry. The slurry was casted on Al foil and dried at 90 ^oC under vacuum overnight. The Al foil coated with cathode material was cut to discs (diameter 14 mm). The mass loading of cathode was ca. 6 mg cm^{-2}. The coin cells were assembled in a glove box and there were no liquid electrolytes were added in coin cells.

Chapter 5 Conclusion of the dissertation

Flexible lithium-ion battery system is considered as the requirement of portable /wearable electronic applications development. Designing flexible FIBs with different shapes and fabrication methods could open up a path for flexible device design innovation. Indeed, current flexible LIBs researches are still at very early stage. Nevertheless, with the development of the standards and new materials, the essential technical issues of the current FLIBs shall be solved.

In this dissertation, couple strategies about developing flexible component materials for flexible lithium-ion batteries have been introduced. Started from facile design of cathode material to MOFs incorporated gel electrolyte for flexible lithium-ion batteries. The essential technical issues with current flexible lithium-ion batteries research were focused and uncovered.

We first designed a robust cathode matrix structure by using V_2O_5/CNT composite incorporated with PTFE framework. PTFE obtains amongst the highest resistivity of any material that is insoluble in lithium-ion battery solvents. While V_2O_5/CNT frameworks might still break into fracture, small amount of PTFE directly formed a network structure within the composite after

heating, provides exceptional high mechanical strength without unnecessary loss of the capacity. The concept of designing composite material and fabrication method was proposed and demonstrated. A high stress resistance (11.2MPa), superior young's modulus (~ 800), and its increased toughness (from 18.2×10^4 J m^{-3} before hot press to 103.1×10^4 J m^{-3} after hot press), provides an advanced standard for FLIBs electrode materials.

In addition, we revealed that the lithium-ion conduction could be exclusively promoted in gel polymer electrolytes by metal-organic framework (MOF) fillers. Gel polymer electrolyte was considered as best candidate for flexible battery system because it exhibits higher ionic conductivity than conventional liquid electrolyte and most importantly, better battery safety. The optimum design of the MOF incorporated gel polymer was achieved by employed functional UiO-66 nanoparticles as the filler and PVDF-HFP as the host to construct a new hybrid membrane. The tuning of ionic transport is realized by the interaction between anions and unsaturated OMS of UiO-66. This specific chemical regulation of ions enables high Li^+ transport efficiency and good interface electrochemical stability, thus leading to promising electrochemical performance in gel polymer electrolytes. As a result, both LMBs and LIBs exhibit outstanding battery performance.

Above works provided new strategies for design and improve the battery component materials in FLIBs with facile and cost-effective way. The methodology we proposed opens new path for designing FLIBs and hopefully lead to new innovations.

Charpter 6 reference

1. The World Counts. https://www.theworldcounts.com/challenges/climate-change/energy.

2. BP statistical review of world energy 2020, 69th edition. *https://www.bp.com/content/dam/bp/business-sites/en/global/corporate/pdfs/energy-economics/statistical-review/bp-stats-review-2020-full-report.pdf*.

3. Collins, J.; Gourdin, G.; Foster, M.; Qu, D., Carbon surface functionalities and SEI formation during Li intercalation. *Carbon* **2015,** *92*, 193-244.

4. Linden, D., Handbook of batteries and fuel cells. *mgh* **1984**.

5. Choi, J. W.; Aurbach, D., Promise and reality of post-lithium-ion batteries with high energy densities. *Nature Reviews Materials* **2016,** *1* (4), 1-16.

6. Dresselhaus, M.; Thomas, I., Alternative energy technologies. *Nature* **2001,** *414* (6861), 332-337.

7. Lee, H.; Yanilmaz, M.; Toprakci, O.; Fu, K.; Zhang, X., A review of recent developments in membrane separators for rechargeable lithium-ion batteries. *Energy & Environmental Science* **2014,** *7* (12), 3857-3886.

8. Liu, C.; Neale, Z. G.; Cao, G., Understanding electrochemical potentials of cathode materials in rechargeable batteries. *Materials Today* **2016,** *19* (2), 109-123.

9. Cho, J.; Kim, Y. J.; Park, B., Novel LiCoO2 cathode material with Al2O3 coating for a Li ion cell. *Chemistry of Materials* **2000,** *12* (12), 3788-3791.

10. Islam, M. S.; Fisher, C. A., Lithium and sodium battery cathode materials: computational

insights into voltage, diffusion and nanostructural properties. *Chemical Society Reviews* **2014,** *43* (1), 185-204.

11. Xu, W.; Wang, J.; Ding, F.; Chen, X.; Nasybulin, E.; Zhang, Y.; Zhang, J.-G., Lithium metal anodes for rechargeable batteries. *Energy & Environmental Science* **2014,** *7* (2), 513-537.

12. Yamada, Y.; Usui, K.; Chiang, C. H.; Kikuchi, K.; Furukawa, K.; Yamada, A., General observation of lithium intercalation into graphite in ethylene-carbonate-free superconcentrated electrolytes. *ACS applied materials & interfaces* **2014,** *6* (14), 10892-10899.

13. Teshima, K.; Inagaki, H.; Tanaka, S.; Yubuta, K.; Hozumi, M.; Kohama, K.; Shishido, T.; Oishi, S., Growth of well-developed Li4Ti5O12 crystals by the cooling of a sodium chloride flux. *Crystal growth & design* **2011,** *11* (10), 4401-4405.

14. Chan, M. K.; Wolverton, C.; Greeley, J. P., First principles simulations of the electrochemical lithiation and delithiation of faceted crystalline silicon. *Journal of the American Chemical Society* **2012,** *134* (35), 14362-14374.

15. Xu, K., Nonaqueous liquid electrolytes for lithium-based rechargeable batteries. *Chemical reviews* **2004,** *104* (10), 4303-4418.

16. Gwon, H.; Hong, J.; Kim, H.; Seo, D.-H.; Jeon, S.; Kang, K., Recent progress on flexible lithium rechargeable batteries. *Energy & Environmental Science* **2014,** *7* (2), 538-551.

17. Li, X.; Yang, J.; Hu, Y.; Wang, J.; Li, Y.; Cai, M.; Li, R.; Sun, X., Novel approach toward a binder-free and current collector-free anode configuration: highly flexible nanoporous carbon nanotube electrodes with strong mechanical strength harvesting improved lithium storage. *Journal of Materials Chemistry* **2012,** *22* (36), 18847-18853.

18. Chen, J.; Minett, A. I.; Liu, Y.; Lynam, C.; Sherrell, P.; Wang, C.; Wallace, G. G.,

Direct growth of flexible carbon nanotube electrodes. *Advanced Materials* **2008,** *20* (3), 566-570.

19. Ng, S.; Wang, J.; Guo, Z.; Chen, J.; Wang, G.; Liu, H., Single wall carbon nanotube paper as anode for lithium-ion battery. *Electrochimica Acta* **2005,** *51* (1), 23-28.

20. Li, S.; Luo, Y.; Lv, W.; Yu, W.; Wu, S.; Hou, P.; Yang, Q.; Meng, Q.; Liu, C.; Cheng, H. M., Vertically Aligned Carbon Nanotubes Grown on Graphene Paper as Electrodes in Lithium-Ion Batteries and Dye-Sensitized Solar Cells. *Advanced Energy Materials* **2011,** *1* (4), 486-490.

21. Wang, J.-Z.; Zhong, C.; Chou, S.-L.; Liu, H.-K., Flexible free-standing graphene-silicon composite film for lithium-ion batteries. *Electrochemistry Communications* **2010,** *12* (11), 1467-1470.

22. Zhou, G.; Wang, D.-W.; Hou, P.-X.; Li, W.; Li, N.; Liu, C.; Li, F.; Cheng, H.-M., A nanosized Fe 2 O 3 decorated single-walled carbon nanotube membrane as a high-performance flexible anode for lithium ion batteries. *Journal of Materials Chemistry* **2012,** *22* (34), 17942-17946.

23. Zhang, H. X.; Feng, C.; Zhai, Y. C.; Jiang, K. L.; Li, Q. Q.; Fan, S. S., Cross-stacked carbon nanotube sheets uniformly loaded with SnO2 nanoparticles: a novel binder-free and high-capacity anode material for lithium-ion batteries. *Advanced Materials* **2009,** *21* (22), 2299-2304.

24. Marschilok, A.; Lee, C.-Y.; Subramanian, A.; Takeuchi, K. J.; Takeuchi, E. S., Carbon nanotube substrate electrodes for lightweight, long-life rechargeable batteries. *Energy & Environmental Science* **2011,** *4* (8), 2943-2951.

25. Jia, X.; Yan, C.; Chen, Z.; Wang, R.; Zhang, Q.; Guo, L.; Wei, F.; Lu, Y., Direct growth of flexible LiMn 2 O 4/CNT lithium-ion cathodes. *Chemical Communications* **2011,** *47* (34), 9669-9671.

26. Luo, S.; Wang, K.; Wang, J.; Jiang, K.; Li, Q.; Fan, S., Binder-free LiCoO2/carbon nanotube cathodes for high-performance lithium ion batteries. *Advanced materials* **2012,** *24* (17), 2294-2298.

27. Hu, L.; Cui, Y., Energy and environmental nanotechnology in conductive paper and textiles. *Energy & Environmental Science* **2012,** *5* (4), 6423-6435.

28. Dikin, D. A.; Stankovich, S.; Zimney, E. J.; Piner, R. D.; Dommett, G. H.; Evmenenko, G.; Nguyen, S. T.; Ruoff, R. S., Preparation and characterization of graphene oxide paper. *Nature* **2007,** *448* (7152), 457-460.

29. Abouimrane, A.; Compton, O. C.; Amine, K.; Nguyen, S. T., Non-annealed graphene paper as a binder-free anode for lithium-ion batteries. *The Journal of Physical Chemistry C* **2010,** *114* (29), 12800-12804.

30. Zhao, X.; Hayner, C. M.; Kung, M. C.; Kung, H. H., Flexible holey graphene paper electrodes with enhanced rate capability for energy storage applications. *ACS nano* **2011,** *5* (11), 8739-8749.

31. Hu, Y.; Li, X.; Wang, J.; Li, R.; Sun, X., Free-standing graphene–carbon nanotube hybrid papers used as current collector and binder free anodes for lithium ion batteries. *Journal of power sources* **2013,** *237*, 41-46.

32. Liu, F.; Song, S.; Xue, D.; Zhang, H., Folded structured graphene paper for high performance electrode materials. *Advanced Materials* **2012,** *24* (8), 1089-1094.

33. Kim, S. W.; Seo, D. H.; Gwon, H.; Kim, J.; Kang, K., Fabrication of FeF3 nanoflowers on CNT branches and their application to high power lithium rechargeable batteries. *Advanced Materials* **2010,** *22* (46), 5260-5264.

34. Wang, Y.; Cao, G., Developments in nanostructured cathode materials for high-performance

lithium-ion batteries. *Advanced materials* **2008,** *20* (12), 2251-2269.

35. Gwon, H.; Kim, H.-S.; Lee, K. U.; Seo, D.-H.; Park, Y. C.; Lee, Y.-S.; Ahn, B. T.; Kang, K., Flexible energy storage devices based on graphene paper. *Energy & Environmental Science* **2011,** *4* (4), 1277-1283.

36. Chen, Z.; Ren, W.; Gao, L.; Liu, B.; Pei, S.; Cheng, H.-M., Three-dimensional flexible and conductive interconnected graphene networks grown by chemical vapour deposition. *Nature materials* **2011,** *10* (6), 424-428.

37. Ji, H.; Zhang, L.; Pettes, M. T.; Li, H.; Chen, S.; Shi, L.; Piner, R.; Ruoff, R. S., Ultrathin graphite foam: a three-dimensional conductive network for battery electrodes. *Nano letters* **2012,** *12* (5), 2446-2451.

38. Li, N.; Chen, Z.; Ren, W.; Li, F.; Cheng, H.-M., Flexible graphene-based lithium ion batteries with ultrafast charge and discharge rates. *Proceedings of the National Academy of Sciences* **2012,** *109* (43), 17360-17365.

39. Liu, B.; Zhang, J.; Wang, X.; Chen, G.; Chen, D.; Zhou, C.; Shen, G., Hierarchical three-dimensional ZnCo2O4 nanowire arrays/carbon cloth anodes for a novel class of high-performance flexible lithium-ion batteries. *Nano letters* **2012,** *12* (6), 3005-3011.

40. Kara Evanoff†‡, J. B., Mark Schauer§, Igor Kovalenko†, David Lashmore§, W. Jud Ready†‡, and Gleb Yushin†*, Ultra Strong Silicon-Coated Carbon Nanotube Nonwoven Fabric as a Multifunctional Lithium-Ion Battery Anode. *ACS nano* **2012**.

41. Shen, L., et al, Advanced Energy-Storage Architectures Composed of Spinel Lithium Metal Oxide Nanocrystal on Carbon Textiles. *Advanced Energy Materials* **2013**.

42. Tao, T.; Lu, S.; Chen, Y., A Review of Advanced Flexible Lithium-Ion Batteries. *Advanced Materials Technologies* **2018,** *3* (9), 1700375.

43. Fergus, J. W., Ceramic and polymeric solid electrolytes for lithium-ion batteries. *Journal of Power Sources* **2010,** *195* (15), 4554-4569.

44. Quartarone, E.; Mustarelli, P., Electrolytes for solid-state lithium rechargeable batteries: recent advances and perspectives. *Chemical Society Reviews* **2011,** *40* (5), 2525-2540.

45. Stephan, A. M., Review on gel polymer electrolytes for lithium batteries. *European polymer journal* **2006,** *42* (1), 21-42.

46. Agrawal, R.; Pandey, G., Solid polymer electrolytes: materials designing and all-solid-state battery applications: an overview. *Journal of Physics D: Applied Physics* **2008,** *41* (22), 223001.

47. Tarascon, J.-M.; Gozdz, A.; Schmutz, C.; Shokoohi, F.; Warren, P., Performance of Bellcore's plastic rechargeable Li-ion batteries. *Solid State Ionics* **1996,** *86*, 49-54.

48. Saunier, J.; Alloin, F.; Sanchez, J.-Y.; Caillon, G., Thin and flexible lithium-ion batteries: investigation of polymer electrolytes. *Journal of power sources* **2003,** *119*, 454-459.

49. Appetecchi, G.; Scrosati, B., A lithium ion polymer battery. *Electrochimica acta* **1998,** *43* (9), 1105-1107.

50. Lee, S.-Y.; Choi, K.-H.; Choi, W.-S.; Kwon, Y. H.; Jung, H.-R.; Shin, H.-C.; Kim, J. Y., Progress in flexible energy storage and conversion systems, with a focus on cable-type lithium-ion batteries. *Energy & Environmental Science* **2013,** *6* (8), 2414-2423.

51. Kwon, Y. H.; Woo, S. W.; Jung, H. R.; Yu, H. K.; Kim, K.; Oh, B. H.; Ahn, S.; Lee, S. Y.; Song, S. W.; Cho, J., Cable-type flexible lithium ion battery based on hollow multi-helix electrodes. *Advanced Materials* **2012,** *24* (38), 5192-5197.

52. Kwon, Y. H.; Woo, S. W.; Jung, H. R.; Yu, H. K.; Kim, K.; Oh, B. H.; Ahn, S.; Lee, S. Y.; Song, S. W.; Cho, J., Batteries: Cable-Type Flexible Lithium Ion Battery Based on Hollow Multi-Helix Electrodes (Adv. Mater. 38/2012). *Advanced Materials* **2012,** *24* (38), 5145-

5145.

53. Xiao, L.; Chen, Z.; Feng, C.; Liu, L.; Bai, Z.-Q.; Wang, Y.; Qian, L.; Zhang, Y.; Li, Q.; Jiang, K., Flexible, stretchable, transparent carbon nanotube thin film loudspeakers. *Nano letters* **2008,** *8* (12), 4539-4545.

54. Wu, H.; Kong, D.; Ruan, Z.; Hsu, P.-C.; Wang, S.; Yu, Z.; Carney, T. J.; Hu, L.; Fan, S.; Cui, Y., A transparent electrode based on a metal nanotrough network. *Nature nanotechnology* **2013,** *8* (6), 421-425.

55. Lee, J.-Y.; Connor, S. T.; Cui, Y.; Peumans, P., Semitransparent organic photovoltaic cells with laminated top electrode. *Nano letters* **2010,** *10* (4), 1276-1279.

56. Hecht, D. S.; Hu, L.; Irvin, G., Emerging transparent electrodes based on thin films of carbon nanotubes, graphene, and metallic nanostructures. *Advanced materials* **2011,** *23* (13), 1482-1513.

57. Yang, Y.; Jeong, S.; Hu, L.; Wu, H.; Lee, S. W.; Cui, Y., Transparent lithium-ion batteries. *Proceedings of the National Academy of Sciences* **2011,** *108* (32), 13013-13018.

58. Sekitani, T.; Someya, T., Stretchable, large-area organic electronics. *Advanced Materials* **2010,** *22* (20), 2228-2246.

59. Kim, D. H.; Xiao, J.; Song, J.; Huang, Y.; Rogers, J. A., Stretchable, curvilinear electronics based on inorganic materials. *Advanced Materials* **2010,** *22* (19), 2108-2124.

60. Yan, C.; Wang, X.; Cui, M.; Wang, J.; Kang, W.; Foo, C. Y.; Lee, P. S., Stretchable silver-zinc batteries based on embedded nanowire elastic conductors. *Advanced Energy Materials* **2014,** *4* (5), 1301396.

61. Zhang, Y.; Jiao, Y.; Liao, M.; Wang, B.; Peng, H., Carbon nanomaterials for flexible lithium ion batteries. *Carbon* **2017,** *124*, 79-88.

62. Ihsan, M.; Meng, Q.; Li, L.; Li, D.; Wang, H.; Seng, K. H.; Chen, Z.; Kennedy,

S. J.; Guo, Z.; Liu, H.-K., V2O5/mesoporous carbon composite as a cathode material for lithium-ion batteries. *Electrochimica Acta* **2015,** *173*, 172-177.

63. Nitta, N.; Wu, F.; Lee, J. T.; Yushin, G., Li-ion battery materials: present and future. *Materials today* **2015,** *18* (5), 252-264.

64. Dewangan, K.; Sinha, N. N.; Chavan, P. G.; Sharma, P. K.; Pandey, A. C.; More, M.; Joag, D.; Munichandraiah, N.; Gajbhiye, N., Synthesis and characterization of self-assembled nanofiber-bundles of V2O5: their electrochemical and field emission properties. *Nanoscale* **2012,** *4* (2), 645-651.

65. Li, Z.; Liu, G.; Guo, M.; Ding, L.-X.; Wang, S.; Wang, H., Electrospun porous vanadium pentoxide nanotubes as a high-performance cathode material for lithium-ion batteries. *Electrochimica Acta* **2015,** *173*, 131-138.

66. Jia, X.; Zhang, L.; Zhang, R.; Lu, Y.; Wei, F., Carbon nanotube-penetrated mesoporous V 2 O 5 microspheres as high-performance cathode materials for lithium-ion batteries. *RSC Advances* **2014,** *4* (40), 21018-21022.

67. Yan, B.; Li, X.; Bai, Z.; Zhao, Y.; Dong, L.; Song, X.; Li, D.; Langford, C.; Sun, X., Crumpled reduced graphene oxide conformally encapsulated hollow V2O5 nano/microsphere achieving brilliant lithium storage performance. *Nano Energy* **2016,** *24*, 32-44.

68. Fu, K. K.; Cheng, J.; Li, T.; Hu, L., Flexible batteries: From mechanics to devices. *ACS Energy Letters* **2016,** *1* (5), 1065-1079.

69. Jia, X.; Chen, Z.; Suwarnasarn, A.; Rice, L.; Wang, X.; Sohn, H.; Zhang, Q.; Wu, B. M.; Wei, F.; Lu, Y., High-performance flexible lithium-ion electrodes based on robust network architecture. *Energy & Environmental Science* **2012,** *5* (6), 6845-6849.

70. Harris, K. L.; Pitenis, A. A.; Sawyer, W. G.; Krick, B. A.; Blackman, G. S.; Kasprzak,

D. J.; Junk, C. P., PTFE tribology and the role of mechanochemistry in the development of protective surface films. *Macromolecules* **2015,** *48* (11), 3739-3745.

71. Kurzweil, P., Capacitors| electrochemical double-layer capacitors: carbon materials. **2009**.

72. Zhou, W.; Wang, S.; Li, Y.; Xin, S.; Manthiram, A.; Goodenough, J. B., Plating a dendrite-free lithium anode with a polymer/ceramic/polymer sandwich electrolyte. *Journal of the American Chemical Society* **2016,** *138* (30), 9385-9388.

73. Goodenough, J. B.; Kim, Y., Challenges for rechargeable Li batteries. *Chemistry of materials* **2010,** *22* (3), 587-603.

74. Janek, J.; Zeier, W. G., A solid future for battery development. *Nature Energy* **2016,** *1* (9), 1-4.

75. Xu, K., Electrolytes and interphases in Li-ion batteries and beyond. *Chemical reviews* **2014,** *114* (23), 11503-11618.

76. Nair, J. R.; Imholt, L.; Brunklaus, G.; Winter, M., Lithium metal polymer electrolyte batteries: opportunities and challenges. *Electrochemical Society Interface* **2019,** *28* (2), 55.

77. Croce, F.; Appetecchi, G.; Persi, L.; Scrosati, B., Nanocomposite polymer electrolytes for lithium batteries. *Nature* **1998,** *394* (6692), 456-458.

78. Li, Z.; Su, G.; Gao, D.; Wang, X.; Li, X., Effect of Al2O3 nanoparticles on the electrochemical characteristics of P (VDF-HFP)-based polymer electrolyte. *Electrochimica acta* **2004,** *49* (26), 4633-4639.

79. Croce, F.; Persi, L.; Scrosati, B.; Serraino-Fiory, F.; Plichta, E.; Hendrickson, M., Role of the ceramic fillers in enhancing the transport properties of composite polymer electrolytes. *Electrochimica Acta* **2001,** *46* (16), 2457-2461.

80. Fu, X.; Yu, D.; Zhou, J.; Li, S.; Gao, X.; Han, Y.; Qi, P.; Feng, X.; Wang, B.,

Inorganic and organic hybrid solid electrolytes for lithium-ion batteries. *CrystEngComm* **2016,** *18* (23), 4236-4258.

81. Cheng, X.; Pan, J.; Zhao, Y.; Liao, M.; Peng, H., Gel polymer electrolytes for electrochemical energy storage. *Advanced Energy Materials* **2018,** *8* (7), 1702184.

82. Zhu, K.; Liu, Y.; Liu, J., A fast charging/discharging all-solid-state lithium ion battery based on PEO-MIL-53 (Al)-LiTFSI thin film electrolyte. *RCS Adv.* **2014,** *4* (80), 42278-42284.

83. Suriyakumar, S.; Kanagaraj, M.; Angulakshmi, N.; Kathiresan, M.; Nahm, K. S.; Walkowiak, M.; Wasiński, K.; Półrolniczak, P.; Stephan, A. M., Charge–discharge studies of all-solid-state Li/LiFePO 4 cells with PEO-based composite electrolytes encompassing metal organic frameworks. *RCS Adv.* **2016,** *6* (99), 97180-97186.

84. Yuan, C.; Li, J.; Han, P.; Lai, Y.; Zhang, Z.; Liu, J., Enhanced electrochemical performance of poly (ethylene oxide) based composite polymer electrolyte by incorporation of nano-sized metal-organic framework. *J. Power Sources* **2013,** *240*, 653-658.

85. Angulakshmi, N.; Kumar, R. S.; Kulandainathan, M. A.; Stephan, A. M., Composite polymer electrolytes encompassing metal organic frame works: a new strategy for all-solid-state lithium batteries. *J. Phys. Chem. C* **2014,** *118* (42), 24240-24247.

86. Bai, P.; Li, J.; Brushett, F. R.; Bazant, M. Z., Transition of lithium growth mechanisms in liquid electrolytes. *Energy Environ. Sci.* **2016,** *9* (10), 3221-3229.

87. Huo, H.; Wu, B.; Zhang, T.; Zheng, X.; Ge, L.; Xu, T.; Guo, X.; Sun, X., Anion-immobilized polymer electrolyte achieved by cationic metal-organic framework filler for dendrite-free solid-state batteries. *Energy Storage Materials* **2019,** *18*, 59-67.

88. Katz, M. J.; Brown, Z. J.; Colon, Y. J.; Siu, P. W.; Scheidt, K. A.; Snurr, R. Q.; Hupp, J. T.; Farha, O. K., A facile synthesis of UiO-66, UiO-67 and their derivatives. *Chem.*

Commun. **2013,** *49* (82), 9449-9451.

89. Cavka, J. H.; Jakobsen, S.; Olsbye, U.; Guillou, N.; Lamberti, C.; Bordiga, S.; Lillerud, K. P., A new zirconium inorganic building brick forming metal organic frameworks with exceptional stability. *J. Am. Chem. Soc.* **2008,** *130* (42), 13850-13851.

90. Shen, L.; Wu, H. B.; Liu, F.; Zhang, C.; Ma, S.; Le, Z.; Lu, Y., Anchoring anions with metal–organic framework-functionalized separators for advanced lithium batteries. *Nanoscale Hori.* **2019,** *4* (3), 705-711.

91. Tarascon, J. M.; Gozdz, A. S.; Schmutz, C.; Shokoohi, F.; Warren, P. C., Performance of Bellcore's Plastic Rechargeable Li-Ion Batteries. *Solid State Ionics* **1996,** *86-8*, 49-54.

92. Valenzano, L.; Civalleri, B.; Chavan, S.; Bordiga, S.; Nilsen, M. H.; Jakobsen, S.; Lillerud, K. P.; Lamberti, C., Disclosing the Complex Structure of UiO-66 Metal Organic Framework: A Synergic Combination of Experiment and Theory. *Chem. Mater.* **2011,** *23* (7), 1700-1718.

93. Shen, L.; Wu, H. B.; Liu, F.; Brosmer, J. L.; Shen, G.; Wang, X.; Zink, J. I.; Xiao, Q.; Cai, M.; Wang, G., Creating Lithium-Ion Electrolytes with Biomimetic Ionic Channels in Metal–Organic Frameworks. *Adv. Mater.* **2018,** *30* (23), 1707476.

94. Evans, J.; Vincent, C. A.; Bruce, P. G., Electrochemical measurement of transference numbers in polymer electrolytes. *Polymer* **1987,** *28* (13), 2324-2328.

95. Xiao, W.; Li, X.; Guo, H.; Wang, Z.; Zhang, Y.; Zhang, X., Preparation of core–shell structural single ionic conductor SiO2@ Li+ and its application in PVDF–HFP-based composite polymer electrolyte. *Electrochim. Acta* **2012,** *85*, 612-621.

96. Zhang, Z.; You, J. H.; Zhang, S. J.; Wang, C. W.; Zhou, Y.; Li, J. T.; Huang, L.; Sun, S. G., Metal Organic Framework Nanorod Doped Solid Polymer Electrolyte with Decreased

Crystallinity for High-Performance All-Solid-State Lithium Batteries. *ChemElectroChem* **2020**.

97. Zhang, Z.; Huang, Y.; Gao, H.; Hang, J.; Li, C.; Liu, P., MOF-derived ionic conductor enhancing polymer electrolytes with superior electrochemical performances for all solid lithium metal batteries. *Journal of Membrane Science* **2020,** *598*, 117800.

98. Zhu, F.; Bao, H.; Wu, X.; Tao, Y.; Qin, C.; Su, Z.; Kang, Z., High-Performance Metal–Organic Framework-Based Single Ion Conducting Solid-State Electrolytes for Low-Temperature Lithium Metal Batteries. *ACS Appl. Mater. Interfaces* **2019,** *11* (46), 43206-43213.

99. Wu, J.-F.; Guo, X., MOF-derived nanoporous multifunctional fillers enhancing the performances of polymer electrolytes for solid-state lithium batteries. *J. Mater. Chem. A* **2019,** *7* (6), 2653-2659.

100. Han, D.-D.; Wang, Z.-Y.; Pan, G.-L.; Gao, X.-P., Metal–Organic-Framework-Based Gel Polymer Electrolyte with Immobilized Anions To Stabilize a Lithium Anode for a Quasi-Solid-State Lithium–Sulfur Battery. *ACS Appl. Mater. Interfaces* **2019,** *11* (20), 18427-18435.

101. Wang, Z.; Tan, R.; Wang, H.; Yang, L.; Hu, J.; Chen, H.; Pan, F., A Metal–Organic-Framework-Based Electrolyte with Nanowetted Interfaces for High-Energy-Density Solid-State Lithium Battery. *Adv. Mater.* **2018,** *30* (2), 1704436.

102. Kumar, R. S.; Raja, M.; Kulandainathan, M. A.; Stephan, A. M., Metal organic framework-laden composite polymer electrolytes for efficient and durable all-solid-state-lithium batteries. *RCS Adv.* **2014,** *4* (50), 26171-26175.

103. Gerbaldi, C.; Nair, J. R.; Kulandainathan, M. A.; Kumar, R. S.; Ferrara, C.; Mustarelli, P.; Stephan, A. M., Innovative high performing metal organic framework (MOF)-laden nanocomposite polymer electrolytes for all-solid-state lithium batteries. *Journal of Materials Chemistry A* **2014,** *2* (26), 9948-9954.

104. Li, S.; Bin, W. H.; Fang, L.; L., B. J.; Gurong, S.; Xiaofeng, W.; I., Z. J.; Qiangfeng, X.; Mei, C.; Ge, W.; Yunfeng, L.; Bruce, D., Creating Lithium-Ion Electrolytes with Biomimetic Ionic Channels in Metal–Organic Frameworks. *Adv. Mater.* **2018,** *0* (0), 1707476.

105. Wanakule, N. S.; Virgili, J. M.; Teran, A. A.; Wang, Z.-G.; Balsara, N. P., Thermodynamic Properties of Block Copolymer Electrolytes Containing Imidazolium and Lithium Salts. *Macromolecules* **2010,** *43* (19), 8282-8289.

106. Ziqi, W.; Rui, T.; Hongbin, W.; Luyi, Y.; Jiangtao, H.; Haibiao, C.; Feng, P., A Metal–Organic-Framework-Based Electrolyte with Nanowetted Interfaces for High-Energy-Density Solid-State Lithium Battery. *Adv. Mater.* **2018,** *30* (2), 1704436.

107. Choudhury, S.; Mangal, R.; Agrawal, A.; Archer, L. A., A highly reversible room-temperature lithium metal battery based on crosslinked hairy nanoparticles. *Nat. Commun.* **2015,** *6*.

108. Zhu, L.; Zhu, P.; Fang, Q.; Jing, M.; Shen, X.; Yang, L., A novel solid PEO/LLTO-nanowires polymer composite electrolyte for solid-state lithium-ion battery. *Electrochim. Acta* **2018,** *292*, 718-726.

109. Liu, W.; Liu, N.; Sun, J.; Hsu, P.-C.; Li, Y.; Lee, H.-W.; Cui, Y., Ionic Conductivity Enhancement of Polymer Electrolytes with Ceramic Nanowire Fillers. *Nano Lett.* **2015,** *15* (4), 2740-2745.

110. Li, L.; Yang, X.; Li, J.; Xu, Y., A novel and shortcut method to prepare ionic liquid gel polymer electrolyte membranes for lithium-ion battery. *Ionics* **2018,** *24* (3), 735-741.

111. Fu, K.; Gong, Y. H.; Dai, J. Q.; Gong, A.; Han, X. G.; Yao, Y. G.; Wang, C. W.; Wang, Y. B.; Chen, Y. N.; Yan, C. Y.; Li, Y. J.; Wachsman, E. D.; Hu, L. B., Flexible, solid-state, ion-conducting membrane with 3D garnet nanofiber networks for lithium batteries. *Proc.*

Natl. Acad. Sci. U. S. A. **2016,** *113* (26), 7094-7099.

112. Zhao, C.-Z.; Zhang, X.-Q.; Cheng, X.-B.; Zhang, R.; Xu, R.; Chen, P.-Y.; Peng, H.-J.; Huang, J.-Q.; Zhang, Q., An anion-immobilized composite electrolyte for dendrite-free lithium metal anodes. *Proc. Natl. Acad. Sci. U. S. A.* **2017**, 201708489.

113. Zhang, X.; Liu, T.; Zhang, S.; Huang, X.; Xu, B.; Lin, Y.; Xu, B.; Li, L.; Nan, C.-W.; Shen, Y., Synergistic Coupling Between Li6. 75La3Zr1. 75Ta0. 25O12 and Poly (vinylidene fluoride) Induces High Ionic Conductivity, Mechanical Strength and Thermal Stability of Solid Composite Electrolytes. *J. Am. Chem. Soc.* **2017**.

114. Yuan, C.; Li, J.; Han, P.; Lai, Y.; Zhang, Z.; Liu, J., Enhanced electrochemical performance of poly(ethylene oxide) based composite polymer electrolyte by incorporation of nano-sized metal-organic framework. *J. Power Sources* **2013,** *240*, 653-658.

115. Dutta, R.; Kumar, A., Ion transport dynamics in ionic liquid incorporated CuBTC–metal-organic framework based composite polymer electrolyte. *Journal of Materials Science: Materials in Electronics* **2019,** *30* (2), 1117-1132.

116. Zhang, Z.; You, J.-H.; Zhang, S.-J.; Wang, C.-W.; Zhou, Y.; Li, J.-T.; Huang, L.; Sun, S.-G., Metal Organic Framework Nanorod Doped Solid Polymer Electrolyte with Decreased Crystallinity for High-Performance All-Solid-State Lithium Batteries. *ChemElectroChem* **2020,** *7* (5), 1125-1134.

117. Zhu, K.; Liu, Y.; Liu, J., A fast charging/discharging all-solid-state lithium ion battery based on PEO-MIL-53(Al)-LiTFSI thin film electrolyte. *RSC Advances* **2014,** *4* (80), 42278-42284.

118. Suriyakumar, S.; Kanagaraj, M.; Angulakshmi, N.; Kathiresan, M.; Nahm, K. S.; Walkowiak, M.; Wasiński, K.; Półrolniczak, P.; Stephan, A. M., Charge–discharge studies of all-solid-state Li/LiFePO4 cells with PEO-based composite electrolytes encompassing metal

organic frameworks. *RSC Advances* **2016,** *6* (99), 97180-97186.

119. Senthil Kumar, R.; Raja, M.; Anbu Kulandainathan, M.; Manuel Stephan, A., Metal organic framework-laden composite polymer electrolytes for efficient and durable all-solid-state-lithium batteries. *RSC Advances* **2014,** *4* (50), 26171-26175.